

THE LOMONOSOV MOSCOW STATE UNIVERSITY

FINAL REPORT

SPECIAL PROJECT SPC-97-4002

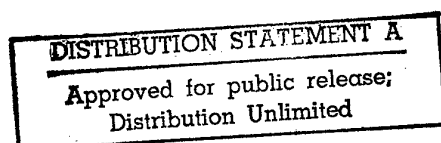
EXPERIMENTAL AND THEORETICAL INVESTIGATION OF DISCHARGE PARAMETERS IN CONDITIONS OF PLASMA AERODYNAMIC EXPERIMENT

Project Principal Investigator

Professor

I.B. Timofeev

DTIC QUALITY INSPECTED 3



19980223 080

REPORT DOCUMENTATION PAGE

Form Approved OMB No. 0704-0188

Public reporting burden for this collection of information is estimated to average 1 hour per response, including the time for reviewing instructions, searching existing data sources, gathering and maintaining the data needed, and completing and reviewing the collection of information. Send comments regarding this burden estimate or any other aspect of this collection of information, including suggestions for reducing this burden to Washington Headquarters Services, Directorate for Information Operations and Reports, 1215 Jefferson Davis Highway, Suite 1204, Arlington, VA 22202-4302, and to the Office of Management and Budget, Paperwork Reduction Project (0704-0188), Washington, DC 20503.

1. AGENCY USE ONLY (Leave blank)

2. REPORT DATE

1998

3. REPORT TYPE AND DATES COVERED

Final Report

4. TITLE AND SUBTITLE

Experimental and Theoretical Investigation of Discharge Parameters in Conditions of Plasma
Aerodynamic Experiment

5. FUNDING NUMBERS

F6170897W0008

6. AUTHOR(S)

Dr. Igor Timofeev

7. PERFORMING ORGANIZATION NAME(S) AND ADDRESS(ES)

Moscow State University
Vorobiovy Gory
Moscow 119899
Russia

8. PERFORMING ORGANIZATION
REPORT NUMBER

N/A

9. SPONSORING/MONITORING AGENCY NAME(S) AND ADDRESS(ES)

EOARD
PSC 802 BOX 14
FPO 09499-0200

10. SPONSORING/MONITORING
AGENCY REPORT NUMBER

SPC 97-4002

11. SUPPLEMENTARY NOTES

12a. DISTRIBUTION/AVAILABILITY STATEMENT

Approved for public release; distribution is unlimited.

12b. DISTRIBUTION CODE

A

13. ABSTRACT (Maximum 200 words)

This report results from a contract tasking Moscow State University as follows: The contractor will investigate plasma discharge parameters as per his 14 Jun 96 proposal, with the exception that the contractor will purchase the equipment himself.

14. SUBJECT TERMS

Fluid Dynamics

15. NUMBER OF PAGES

96

16. PRICE CODE

N/A

17. SECURITY CLASSIFICATION
OF REPORT

UNCLASSIFIED

18. SECURITY CLASSIFICATION
OF THIS PAGE

UNCLASSIFIED

19. SECURITY CLASSIFICATION
OF ABSTRACT

UNCLASSIFIED

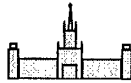
20. LIMITATION OF ABSTRACT

UL

NSN 7540-01-280-5500

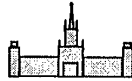
DTIC QUALITY INSPECTED 3

Standard Form 298 (Rev. 2-89)
Prescribed by ANSI Std. Z39-18
298-102



Contents

1. Introduction	3
1.1. Structure of shock waves in weakly ionized plasma	3
1.2. Heating and relaxation effects	6
1.3. Diagnostics of High Speed Low Temperature Air Plasma	10
2. Experimental Investigation of Plasma in Airflow	12
2. 1. General Features of the Discharge Development in Supersonic Airflow	12
2.2. Spectral Diagnostics of Plasma Parameters	30
2.2.1. A Spectroscopic Method of Measurement of Gas Temperature	30
2.2.2. A Method of Measurement of Vibration Temperature of Molecular Plasma	31
2.2.3. A Set Up for Spectral Diagnostics	33
2.2.4. Experimental Results	33
2.3. Probe Plasma Diagnostics	42
3. Theoretical Studies of Supersonic Discharge Physics	45
3.1. General Consideration	45
3.2. Simulation of Plasma Kinetic Processes	62
3.3. Plasma dynamics and current distribution at discharges in flow over a body	73
4. General Consideration of Results	84
5. Conclusions	88
References	90



1. Introduction

Plasma effect on ambient airflow is one of the promising directions of research in aerodynamics.

Several types of gas discharges in airflow have been studied from the viewpoint of possible application in aerodynamics. Those are: longitudinal (i.e. electric current \mathbf{j} is parallel to the airflow velocity \mathbf{v}) and transversal ($\mathbf{j} \perp \mathbf{v}$) DC discharges [1-9], capacity type high frequency discharge [10,11], microwave discharge [12], and optical discharge (laser spark) [13-14].

Among the questions of interest for this application one can mention:

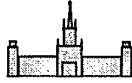
- general flow structure;
- distribution of pressure and tangent viscous forces exerted upon a body that produce drag, thrust, flight control forces, etc.;
- structure and properties of shock waves and precursors;
- heating and relaxation effects;
- consideration of possible ways of plasma application in aerodynamics.

1.1. Structure of shock waves in weakly ionized plasma

At propagation of shock waves in a discharge plasma, both discharge and shock properties are subject to considerable changes.

One of possible mechanisms of such interaction in a weakly ionized non-equilibrium plasma is bound with generation of ion-sound waves [17-21].

It is well known that in plasma with $T_e \gg T_i$ (where T_e , T_i are temperatures of electrons and ions, respectively) there exist low frequency ion-sound oscillations, and it is possible to excite the corresponding shock waves. These oscillations and waves result from unanimous movement of electrons and ions (positive and negative charges cannot part due to neutrality of plasma – otherwise enormous electric fields would appear). This movement depends on effective temperature (which is close to T_e) and effective charged particle mass (which is close to ion mass). As $T_e \gg T_i \approx T_g$ (here T_g is the gas temperature), speed of ion-sound waves



is much higher than speed of sound of the gas. Collisions of ions with neutral particles cause dissipation of part of energy of charged component movement through the transfer of momentum to a neutral gas. It may result in both gas heating and acceleration by ion-neutral friction force.

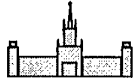
But those effects are considerable only at considerable values of n_i/n , here n_i , n_m are concentrations of ions and neutral particles, i.e. when the plasma is not weakly ionized. That is why one of the greatest deviations (several times) of shock wave speed from the Hugoniot formula due to nonequilibrium effects was observed in hypersonic flows of strongly ionized plasma [16].

In [17,18,20] the structure of flat ion-sound waves of finite amplitude in a weakly ionized plasma, that are excited and maintained by shock waves in a neutral component, was studied theoretically (plasma with one type of ion component was considered). In this case before of a shock wave front there appears rather a long region of disturbance of charged components of plasma, which resembles a shock wave by its form, its width being greater than the mean free paths of ions and neutrals (so called precursor). It was noted that the propagation of shock ion-sound waves in non isothermal electron - positive ion plasma is impossible in absence of external action.

In [19] a shock wave diffusion structure in a non equilibrium plasma of electronegative gases was investigated (this job definition contains additional hydrodynamic equations for one type of negative ions). Contrary to spatial distributions of plasma parameters in the previous cases, a slow decrease of electron concentration in precursor is realized here.

In [21] a precursor in air has been observed at experiments with a high frequency (40 MHz) discharge plasma. At static pressure $p_{st}=10$ Pa; the precursor width was about 3 cm, which coincided with a theoretical result [19].

Another mechanism of precursor formation is associated with non-uniform heating of the gas by electric current (note that heating of electrons by electric current is used in [18-28] to obtain the difference between electron and gas temperatures). If the discharge electric field F

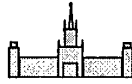


is parallel to the shock wave velocity v_{sw} , it is caused by the field redistribution as a result of changes of the plasma conductivity σ (at gas compression in the shock wave) at constant current density $\mathbf{j} = \sigma \mathbf{F}$. A steady electron concentration (i.e. σ) depends on F and n_m , which both change instantly at sudden compression by the shock wave. The processes of ionization or recombination however are comparatively slow, and n_e fits to the new conditions with a considerable delay. It causes a dependence of the plasma parameters distributions in a vicinity of the shock wave on a sign of $v_{sw}\mathbf{F}$ (the relaxation is determined by either recombination or ionization).

In [22] a shock wave structure has been examined for both parallel and anti-parallel $v_{sw}\mathbf{F}$ experimentally and numerically. Equations for flows of electrons, positive and negative ions were added to the equations of gas dynamics. They took into account processes of ionization, electron-ion and ion-ion recombination, attachment of electrons to molecules of oxygen, and detachment of electrons from negative ions. The experiments and computations for air at initial parameters: molecular concentration $n_m = 1.7 \cdot 10^{18} \text{ cm}^{-3}$, field $F = 1.35 \text{ kV/cm}$, Mach number $M=3$ showed the following. If the direction of field coincides with a direction of the shock wave propagation ($v_{sw}\mathbf{F} > 0$), then before the shock wave there appears a region (about 0.5 cm long) with higher values of F/n_m parameter, and it leads to the higher luminosity of a gas there. Behind the front the values of F/n_m are reduced, and a dark region appears there. At another field direction ($v_{sw}\mathbf{F} < 0$) there can be only a region with reduced F/n_m values behind the front.

In [23] there is developed a theory for the concentrations of charged particles and electric field strength in case of a shock wave propagation in a plasma of longitudinal gas discharge. Estimates for sizes of regions of disturbances near the shock wave front were obtained. Their results are similar to those of [22], with the precursor length $\sim 0.7 \text{ cm}$. It was shown that the character of the disturbance depends on direction of electric current, and is different in case of electropositive and electronegative gases.

Thus, in plasma the characteristic size of the precursor can be sufficiently greater than the width of shock wave front in a neutral gas. However, this size is about a few centimeters

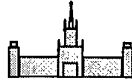


only, and it falls at air pressure gain. It is not easy to find out a realistic situation in which the precursors could affect an aerodynamic flow significantly.

1.2. Heating and relaxation effects

In [1] there was experimentally investigated the propagation of a shock wave through a glow discharge plasma in air. There was fixed an anomalous high velocity of the shock wave. Besides that changes of pressure profile were observed. In [1] there is made an assumption of the vibration relaxation effect, in result of which the energy stored at vibration levels passes to gas heating. But estimates show that a time of vibration relaxation behind the shock wave front are about an order of magnitude greater than the time of shock wave propagation through the discharge region. In this case vibration degrees of freedom stay practically frozen during the experimental time and can not significantly effect on shock wave parameters. This conclusion is made also in [4], where it was noted that it is possible to develop processes analogous to detonation in gases including non equilibrium store of internal energy, but they have a threshold that is determined by a critical diameter d_k . In case of relaxing gas d_k depends on pressure p_{st} ($d_k \sim 1/p_{st}$). Calculations made in [4,34] have shown that the typical size of region of relaxation of vibration energy behind the shock wave front is ~ 10 cm in hydrogen (for initial $p_{st}=10$ Torr, $T_g = 300$ K and $M_0=2$), and several orders of magnitude greater in nitrogen at the same conditions. In experiment [1] the conditions for detonation are not met.

In [5] there was investigated the propagation of the shock wave with Mach numbers $M=1.5-3$ in a plasma of a longitudinal glow discharge at low and high pressures ($p_{st}=1-300$ Torr). There were made the measurements of gas temperature and its distribution over the discharge cross section. It was noted that at low pressures (diffusion or weakly constricted type of discharge) there is observed a good agreement between the experimental data on the shock wave acceleration and calculations of one-dimensional normal fall of the shock wave on an interface of two media with different sound velocities [13]. But at increase of pressure (and input power), i.e. during transition to the constricted conditions, the difference between theory and experiment grew up, and the experimental values of shock wave were higher than the computed ones. Hence the gas discharge non uniformity in the direction transverse to the



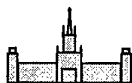
shock wave propagation direction is significant. A more detailed, at least two dimensional approach is to be applied, which takes into account the temperature distribution.

In [9] theoretically (in a two-dimensional formulation of a problem) and experimentally there was studied a shock wave propagation through a plasma of a transverse discharge in air. There was also noted that the increase of wave velocity and the curvature of the front are in a good agreement with the model of shock wave interaction with heat non-uniformity. In [4] a study of the shock wave propagation in a longitudinal discharge in hydrogen and in nitrogen was made. For all the gases it was detected the increase of the mean shock wave propagation at the discharge switching on. In these experimental conditions the increase of the shock wave was mainly determined by heating of a gas. Experimental data fitted well to the calculations on base of one dimensional theory [13].

In a theoretical work [35] there was considered the shock wave movement through a heat non uniformity. For evaluation of the shock wave velocity through the region with non uniform shape of density there was used the approximate method of Witham. A good agreement of the approximate approach with the experiment [36] was observed.

One can see that the acceleration of shock waves can be sometimes explained by gas heating. In these cases practically in all the works a total input of energy into heating was considered. There were practically no works that considered the distribution of energy balance over the discharge volume. For the determination of the heating mechanism it is necessary to have the precise experimental picture of a gas temperature distribution over the discharge region and the corresponding value of F/n_m .

The exchange of energy between the translation and internal degrees of freedom of molecules was considered in a number of works. It was shown that a shock wave can become stronger and have higher velocity due to transformation of vibration energy to the shock wave. In [37] there was considered a two-dimensional interaction of a shock wave with a cylindrical region of a relaxing gas. It was shown that the character of the shock wave propagation substantially depends on Damkeller number $D_a = \tau_g/\tau_{VT}$ that characterises the ratio of characteristic gas dynamic time τ_g and relaxation time τ_{VT} . A comparison was made with



computation results of flat shock wave interaction of the same intensity with a cylindrical region of hot non reacting gas. It was noted that the considered processes of a shock wave interaction with a relaxing gas and a heat non uniformity have some features in common (in spite of qualitative difference). In particular, there takes place a considerable acceleration of the wave front inside the non uniformity region, and it leads to analogous curvature of the front of initial shock wave. In both cases the wave that has already passed the region of non uniformity became considerably weaker. We see that both mechanisms can lead not only to the acceleration of the shock wave, but they can also destroy the flat front of the incident shock wave. It makes difficult an unambiguous interpretation of phenomena in gas discharges with non uniform distribution of temperature and power input.

In a work [37] there were made computations of gas dynamic phenomena of non equilibrium excitation of a spherical air region at different ratios between time period of energy input and characteristic gas dynamic and relaxation time periods. A significance of non equilibrium effects of power output and duration of gas excitation was shown.

In [38] in a one-dimensional formulation there was considered a shock wave propagation through a region of lower density or high vibration temperature. It was noted that in both cases the acceleration of shock wave is observed. Intensity of the shock wave decreases in a region of non uniformity, and it increases in a vibration excited region. In the latter case the shape of pressure has a detonation peak. Shock waves in a gas with excited vibrations can become detonation waves. The importance of works [37,38,15] consists in including of real discharge parameters into the consideration: the share of input energy that goes to vibration states; the redistribution of energy between different types of molecules in air; the change of rate of vibration relaxation in strongly excited gas (what is typical for gas discharges) in comparison with unexcited one.

In a work [40] there was numerically studied a process of propagation of a weak flat shock wave in a vibration excited nitrogen with addition of water vapour (1 and 5%). At the excess of vibration energy in comparison with equilibrium value the shock wave became stronger, and this effect depended on the initial Mach number. The presence of water molecules in a gas mixture can significantly change the effective rate of vibration relaxation [41]. For a

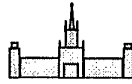


proper description sometimes it is necessary to analyse a model including redistribution of energy between different types of molecules. In a work [42] there was considered the vibration excited region of air discharge with account of such processes and the diffusion of excited molecules to the walls (in harmonic molecular exchange approach). A steady state with high level of vibration excitation, $E_V/E = 1-4$ (where E_V is a discharge energy input to vibrations, E - to translation states) in air discharge can be achieved only in narrow discharge tubes of radius $\sim 1-2$ cm and low pressures ~ 3 Torr, in a wider tubes and at pressures > 10 Torr $E_V/E \leq 1$. So the realisation of vibration-relaxation effects is limited by conditions of real discharge experiments.

The listed results show that almost in most of theoretical models of shock wave propagation in excited molecular gases, besides maybe [15,37, 38], unrealistic conditions were considered. So the obtained theoretical results do not give an unambiguous description of the peculiarities of movement of shock waves in discharge regions.

These studies show that a number of non-equilibrium plasma chemical reactions should be taken into account at consideration of plasma effect on hydrodynamics. One of the most comprehensive lists of types of these reactions is presented in [76]. One of the most detailed computations of air plasma reactions, under conditions similar to those characteristic for plasma aerodynamic experiments, have been produced in [57] together with experimental verification. Some cross sections for air plasma are presented in [76, 57, 25-32].

For some cases (see, e.g., [41]) it is possible to divide the whole problem into two, i.e. to produce a separate preliminary computation of electron distribution function over energy in air discharge. Such computation has been carried out in [24]; humidity was taken into account, the Boltzmann equation was solved numerically in a two-term approximation [25]. These results are very useful if a quasi steady state is achieved (e.g., at glow discharges in a steady air, see above). However consideration with use of this approximation can be unreliable under conditions of present aerodynamic experiments (see below). The characteristic rates of different plasma relaxation processes are of the same orders of magnitude as the process characteristic time (as a rule a steady state is not achieved even during all the lifetime of a plasma mass element in the discharge region). One should not



neglect unsteady non-equilibrium processes that affect the electron distribution function. It is likely to be necessary to produce their direct unsteady computation together with gas dynamic processes and the Maxwell equations. The characteristic values of electric field, electron concentration, and gas temperature are too high, so humidity is unimportant. That is why we have not used this approximation at our further studies (see below).

Thus, we don't know any theoretical works that would consider plasma kinetic processes, discharge structure, and gas dynamical structure under conditions of plasma aerodynamic experiments, and which reliability could be compared with experimental data on plasma parameters. A step in this direction was one of objectives of present studies.

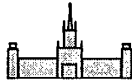
1.3. Diagnostics of High Speed Low Temperature Air Plasma

At the previous experiments on plasma aerodynamics, diagnostic methods were used (photographs and shadow photographs with exposition times that are long in comparison with characteristic time, movies, total voltage and current measurement, total drag etc.) which are as a rule low informative concerning plasma parameters, discharge structures, and basic processes. Basic parameters (distributions of plasma concentration and electron temperature, electric current and field, gas temperature, vibration and electron excitation characteristics, etc.) were practically unknown. It prevented to reveal basic causes of plasma effect on aerodynamics, and to estimate prospects of its optimization for application.

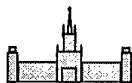
That is why plasma diagnostics under conditions of plasma aerodynamic experiments was a major objective of our present experimental investigation.

At analysis of previous studies of plasma aerodynamics the researchers as a rule assumed that the processes are quasi stationary. Diagnostics of steady plasma is rather traditional, it is described in several monographs.

Note that our present experiments have shown that the results based on this assumption can be unreliable. Even DC discharges in stationary airflow expose various fast movements of plasma channels and changes of macroscopic structure. It does not contradict with other



experimental data available from the literature. It seems that it is caused not only by technical difficulties of model construction optimization and of proper organization of the discharge, but also by instabilities inherent to comparatively powerful discharges in dense electronegative gas like air. Unsteady processes with characteristic time < 1 ms can be studied with use of well developed methods [50-56], but these methods as a rule need considerable modifications to be applied for diagnostics of plasma in supersonic or hypersonic airflow.



2. Experimental Investigation of Plasma in Airflow

2.1. General Features of the Discharge Development in Supersonic Airflow

Experiments on formation and diagnostics of discharges in supersonic airflow volumes near surfaces of models have been carried out. The models for the plasma aerodynamic experiments had been developed by Dr. A.I.Klimov. A schematic draft of the models is presented on fig. 2.1 and 2.3. Each model has a shape of cylinder (1) with a 15° conic and \varnothing 8 mm spherical (2), or a simply conic (3) frontal frustum part, and a spike (4). Each spike had a cylindrical part (a \varnothing 4 mm ceramic tube) (3), and sharp (10°) copper cone (4) on a top. Both models were as a rule made of acrylic plastic, but at some experiments in TsAGI ceramic models were used, to prevent intensive erosion of model surface material during the discharge. Each model had a sectioned electrode composed of eight copper electrodes fixed inside the model's frontal part, they were positioned equidistantly (45°) on one plane normal to the axis of symmetry. The frontal sharp conic part of the model's spike served as another electrode. Its length was 27 mm in both cases.

At aerodynamic experiments the model was positioned along the wind tunnel axis.

Two types of discharge between the frontal spike electrode and the sectioned electrode were used at the plasma aerodynamic experiments.

The first type – direct current (0.5...2.6 A) discharges with input power up to 1.5 kW, with current parallel or anti-parallel in respect to the airflow velocity. A schematic draft of the electric scheme of connection between the electrodes and a power supply source is shown of fig. 2.5. Each of the 8 electrodes E1 (situated on the lateral surface of the model's frontal part) was connected with one of the poles of the power supply source through one of resistors of a group R3 sequentially with resistors R1 and R2 (or with switch blades S1 and S2). The other pole of the power supply unit was joined with the spike electrode. The ballast resistance unit was composed of low induction resistances (TBO type), 60 W each. The resistance unit of the R3 group consisted of 8 equivalent pieces (12.5 k Ω , 25 k Ω or 50 k Ω each). $R1 = R2 = 3$ k Ω . The ballast resistance could vary between 1.56 and 12.23 k Ω .

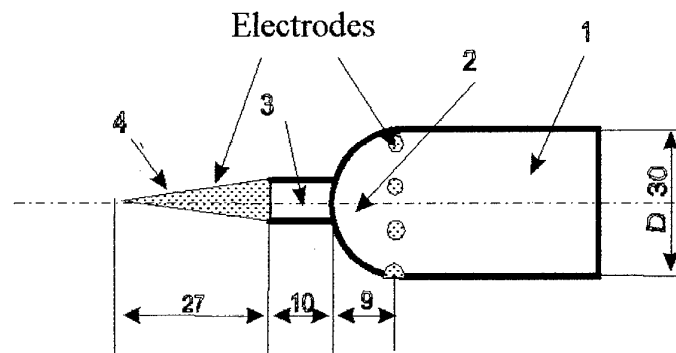
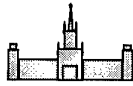


Fig. 2.1. Schematic design of plasma generator with spherical frontal part of the model. The sizes are in mm.

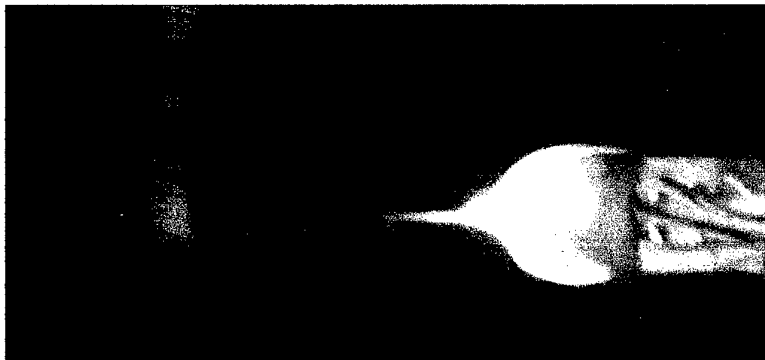


Fig. 2. 2. Appearance of a discharge with the model with spherical frontal part.
 $M = 2.3$, $I = 1.6$ A

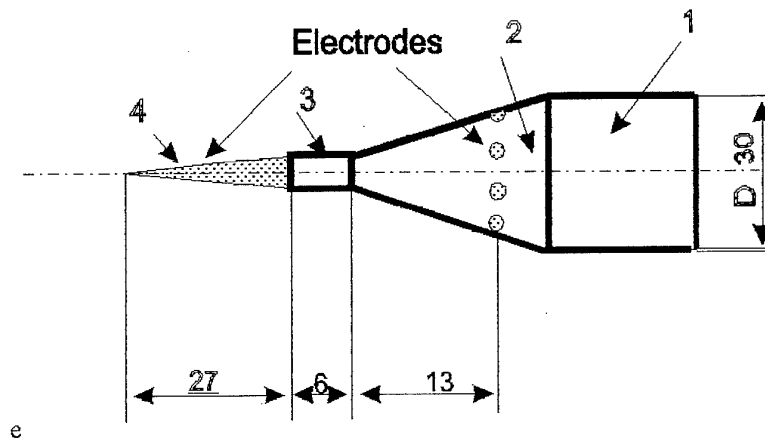
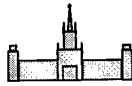


Fig. 2.3. Schematic design of a plasma generator with conic frontal part.
The sizes are in mm.

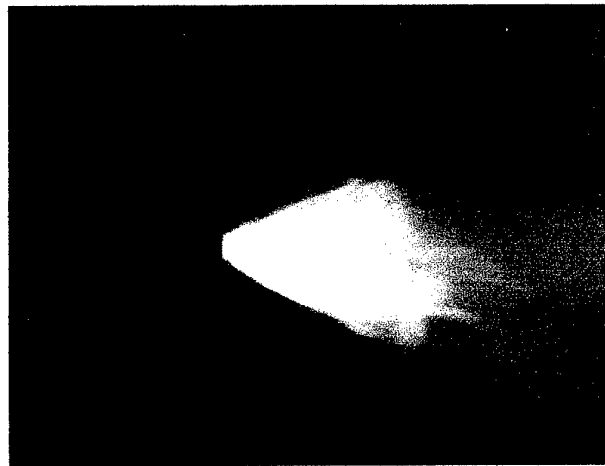


Fig.2.4. Appearance of a discharge with the model with conic frontal part.
 $M = 2.3$, $I = 1.6$ A

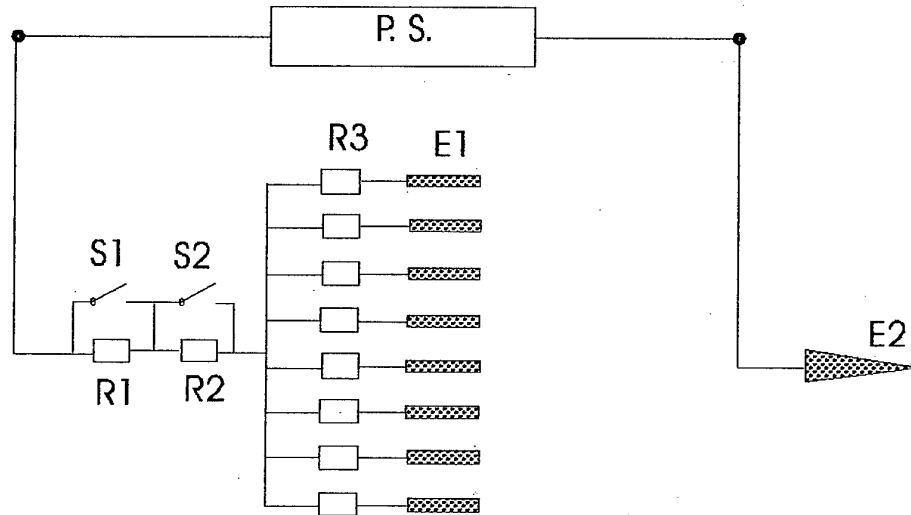
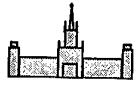


Fig. 2.5. Ballast resistance unit scheme



The power supply unit was composed of capacitors with a nominal voltage $U = 5$ kV and capacity $C = 100$ μ F. The total capacity of the battery amounted to 4,800 μ F, and the total energy store achieved $W = 120$ kJ. The capacity battery was connected with the load by a special discharge switch controlled by application of a high voltage pulse to its interelectrode gap. A characteristic time of the battery's discharge to the load $\tau = RC$ could be varied from 7.5 to 58 s.

The second type – AC discharge with frequency $f = 50$ Hz, the maximal current varied from 0.5 to 5 A (in dependence on experimental conditions) at maximal discharge input power about 0.9 kW.

AC 220 V, 50 Hz network power supply was applied, a high-voltage transformer was used for amplitude voltage build-up to $U_0 = 7$ kV, its secondary high-voltage winding was connected to the discharge gap through a ballast resistance unit (see fig. 2.5).

The discharge investigation was carried out at the following parameters of the ambient airflow: pressure $p_0 = 1$ atm, static pressure $p_{st} = 30$ Torr, Mach number $M = 2.3$, static gas temperature $T_{st} = 160$ K (Dr. Klimov's installation, MRTI); $p_0 = 6$ atm, $p_{st} = 29$ Torr, $M = 3.98$, $T_{st} = 68$ K (TsAGI's wind tunnel).

One should note that the both types of discharge power supply have been tested on the both installations with use of the both types of models (with spherical and conic frontal parts).

The discharge voltage-current characteristics have proved to be practically the same for the $M = 2.3$ MRTI and the $M = 4$ TsAGI experiments. For example, fig.2.6,a presents fragments of voltage (upper curve) and current (lower curve) oscillograms for an AC discharge in steady air (no airflow). One can see that the discharge current over time function $I = I(t)$ is a distorted sine function with considerable (1.5...2 ms) periods of zero current. During these periods a fast growth of the discharge gap voltage is registered: e.g., at $U_0 = 7$ kV, $\partial U/\partial t|_{I(t)=0} = 2.2$ MV/s. As soon as the breakdown voltage is achieved, the discharge gap voltage falls and then holds practically constant (≈ 1 kV) during the next 7...7.5 ms. Maximal current here corresponds to 2.6 A.

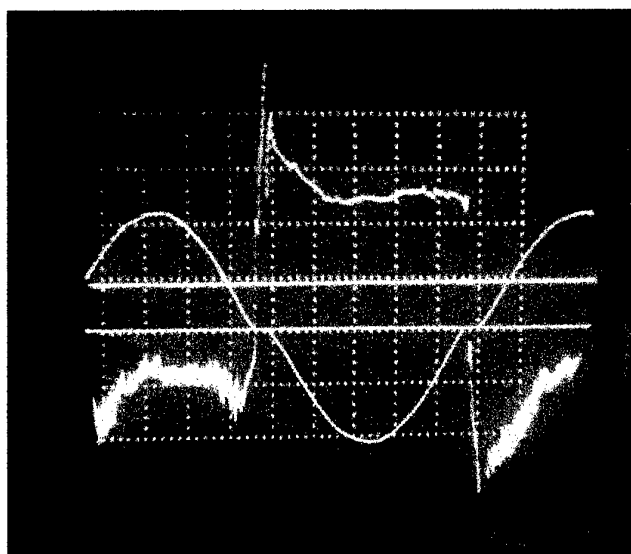
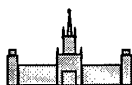
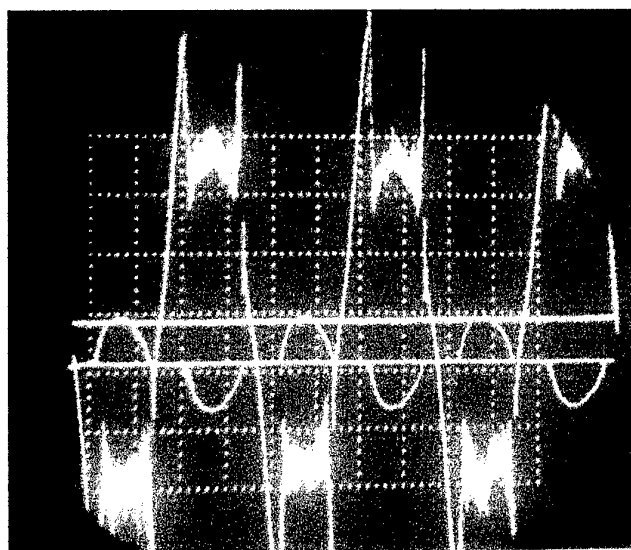
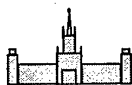
*a)**b)*

Fig. 2.6. A typical appearance of oscillograms of interelectrode gap voltage (upper curves) and discharge current (lower curves): *a)* - without, *b)* - with airflow ($M = 4$, the model with spherical frontal part, AC 2.6 A, maximal power source voltage 5 kV)



Voltage (upper curve) and current (lower curve) oscillograms for an AC discharge in the supersonic airflow at the TsAGI experiments ($M = 4$) are presented on fig. 2.6,b. Their general appearance is similar to that at the discharge in the steady air, but the period of zero current is longer, the breakdown voltage is higher, bell-shaped curves are registered for voltage instead of the horizontal intervals, and high-frequency pickup components have appeared. These high-frequency noise components can result from the following:

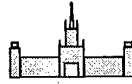
- 1) – unstable behavior of the discharge in the supersonic airflow (discharge current channels can be formed and destroyed, plasma-gas surface can vibrate, vortices can be formed, etc.);
- 2) – local breakdowns in the ballast resistance unit and/or in the connecting wiring (that have been observed during the experiments).

The latter cause looks more probable.

A visual appearance of the DC discharges (at the capacitor power source) is similar to that of the AC discharges. The corresponding voltage and current oscillograms are characteristic for capacitor discharges with high resistance load: the discharge current over time function $I = I(t)$ is a falling exponent with the characteristic time $\tau = RC$ which is determined by the ballast resistance R .

Fig. 2.2 presents a typical DC discharge appearance for the spherical frontal part model in a quasi stationary airflow with a slowly falling speed (from $M = 2.3$ to $M = 1$). These experiments have been carried out with use of Dr. Klimov's installation in MRTI. Maximal current was 1.6 A, and maximal discharge gap voltage 4 kV. The discharge looks to be axisymmetric in general. All the discharge gap is filled by plasma. According to the photo frame, the radiating plasma layer on the model's frontal part can be 2...2.5 mm thick, its borders are rather sharp. The radiation is not uniform, it is especially vividly seen near the hind electrodes. Plasma protuberances are observed downstream the discharge interelectrode gap.

An appearance of an AC discharge in a quasi stationary airflow with a slowly falling speed (from $M = 2.3$ to $M = 1$, Dr. Klimov's installation in MRTI) with the conic frontal part



model is exposed on a fig. 2.4. Maximal current is 1.6 A, discharge voltage bell maximum is $U_1 = 5$ kV, discharge duration time $\tau = 5$ s, photo frame exposition time $\Delta t = 1/30$ s.

One can see that the discharge plasma envelopes all the frontal part of the model, and fills all the interelectrode gap. But, contrary to the previous case, the plasma boarder is not so sharp, some plasma is ejected from the discharge region. Plasma radiation near the hind edge of the frontal spike electrode is much brighter than elsewhere, other maxims of brightness are observed between the hind electrodes. The expected current channels from the spike electrode to these hind electrodes are all but one apparently shunted by transverse channels between the hind electrodes to form a discharge ring around the model. The discharge current seems to pass through one channel from the spike to one of the hind electrodes and then to the other hind electrodes along the ring channel.

A photo frame of appearance of the model with the conic frontal part after the discharge (fig. 2.7) can serve as a substantiation of this fact. One can see tracks of strong erosion on the model's surface, that are situated: 1) – near the joint of the spike electrode with the dielectric part of the model, and 2) – along the circle that passes through the ends of the hind electrodes. There is no axial symmetry of erosion marks: the upper part of the conic surface of the model has eroded much more than all the rest surface. It is likely that the discharge shunting, with sequent formation of the ring discharge happened in this place (after the discharge photo exposition period, here 1/30 s).

The ring discharge formation on the models is more difficult at higher Mach numbers. Besides that, models with ≈ 1 cm longer interelectrode gap were used at the experiments in TsAGI. As a result, at the first series of experiments in TsAGI it has proved to be very difficult to organize the surface discharge on the models made of acrylic plastic.

A full-color photo frame of the discharge in the $M = 4$ airflow, and a photo frame of the same discharge taken through a blue filter, are shown on fig. 2.8. They show that the discharge is formed on the spherical frontal part of the model along the circle that passes through the hind electrodes. It results from a breakdown and ground connection of one of the hind electrodes.

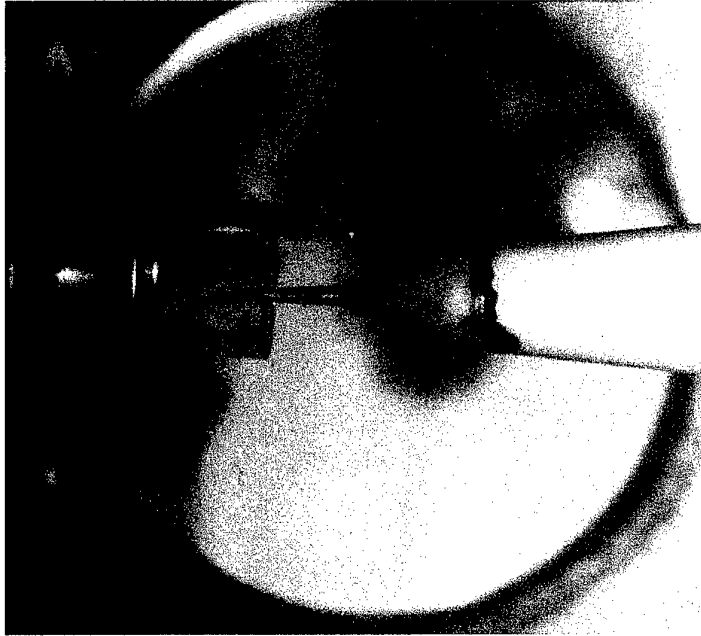
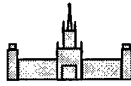


Fig. 2.7. General appearance of a model after one discharge
($M = 2.3$, DC 2.6 A, discharge duration 5 s)

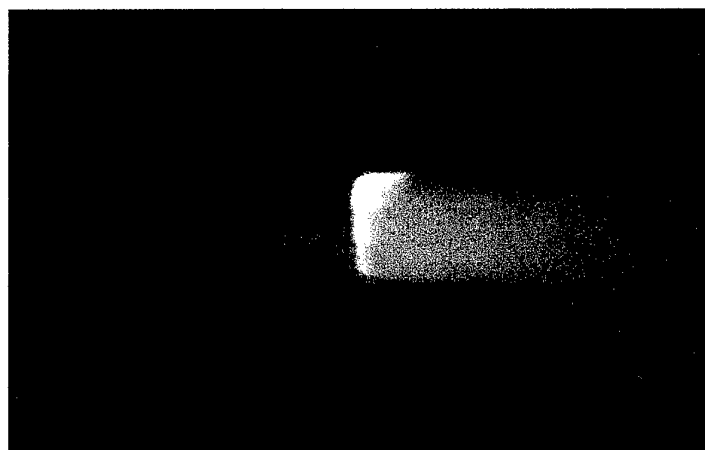
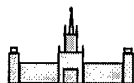
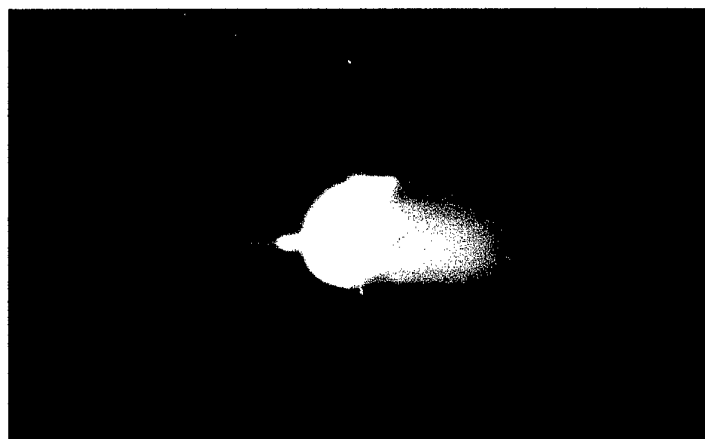
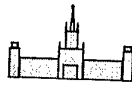
*a)**b)*

Fig. 2.8. A typical appearance of the transversal (ring) discharge ($M = 4$, 2.6 A).
a) - photo frame is taken through a blue filter, *b)* - without any filter



The current and voltage oscillograms that correspond to this regime are all covered by the high frequency noise.

The discharge structure is much more distinct in blue color than on the full-color frame, because the hot regions of the discharge are better seen in this case. As a rule, this discharge regime is accompanied by strong erosion of walls and electrodes, that can result in a considerable degradation of the model's aerodynamic properties. This model cannot be used for further experiments.

Fig. 2.9 illustrates the initial stage of formation of the ring discharge on the model with conic frontal part ($M = 4$). One can easily see the plasma channel that joins some of the hind electrodes. One can also notice a gap with no discharge between two hind electrodes, i.e. their potentials are close to each other. The breakdown and ground connection has probably happened with one or two of the hind electrodes that are situated on the inverse side of the model.

A shortcut in the connecting wiring inside the model itself is perfectly seen on a photo frame presented on fig. 2.10.

All the previous data correspond to models made of acrylic plastic that evaporates easily. But the most successful experiments have been produced with use of models made of refractory ceramics (Fig. 2.11). The discharges on ceramic models with both spherical and conic frontal parts at $M = 4$ cover practically all the surface, but it is still not axisymmetric. For the «spherical» model, one can see a long plasma downstream protuberance being about twice as long as the interelectrode gap (between the frontal spike and the hind electrodes). The «conic» model discharge plasma forms filaments downstream the hind electrodes, that is a result of their rather intensive erosion.

Shadow photo frames of the ring and of the longitudinal (i.e. between the spike and the sectioned hind electrode) discharges in the $M = 4$ airflow are presented on fig. 2.12 and fig. 2.13. Note that the discharge on the model's surface is strongly defocused, that produces an

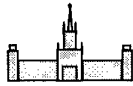


Fig. 2.9. A beginning of the transversal discharge (maximal DC 2.6 A, $M = 4$)

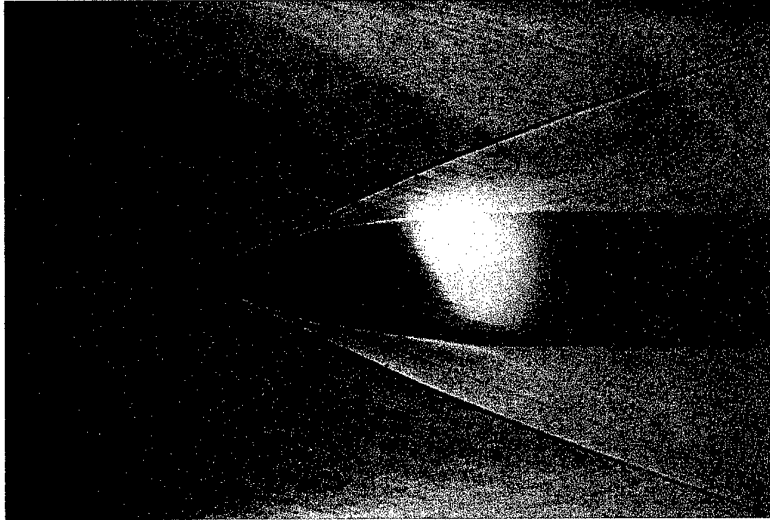
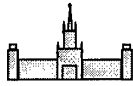


Fig. 2.10. A shortcut inside the model

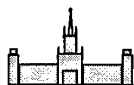
*a)**b)*

Fig.2.11. Discharges over ceramic models with spherical (*a*) and conic (*b*) frontal parts. Maximal current is 2.6 A, maximal power source voltage is 7 kV, $M=4$

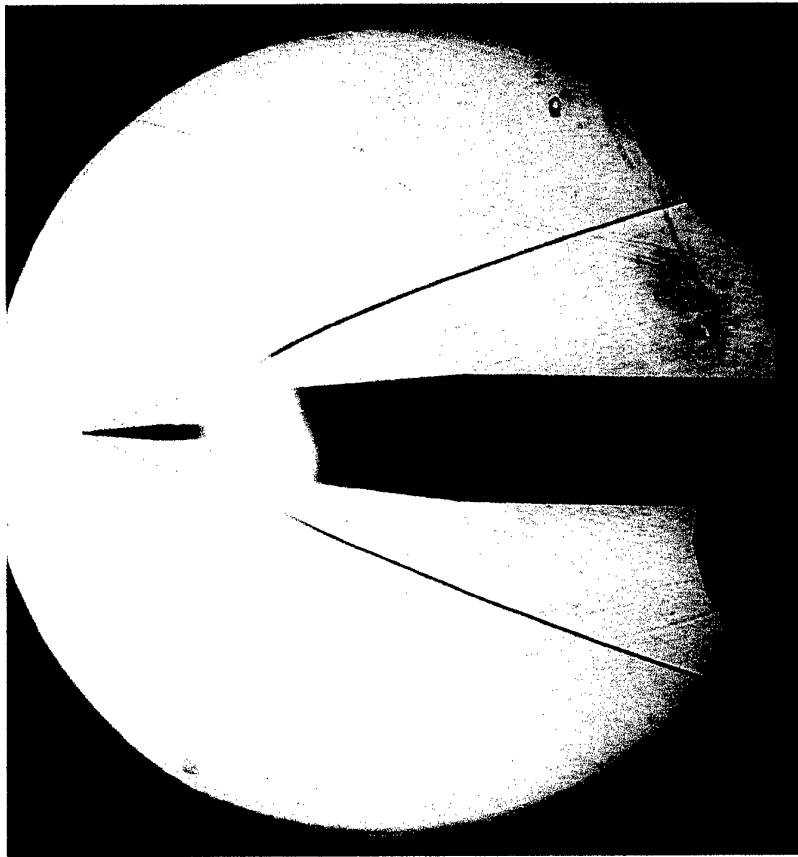
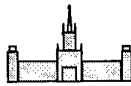


Fig. 2.12. A shadow photo frame of the transversal discharge.
A ceramic model, $M = 4$, DC 1.6 A

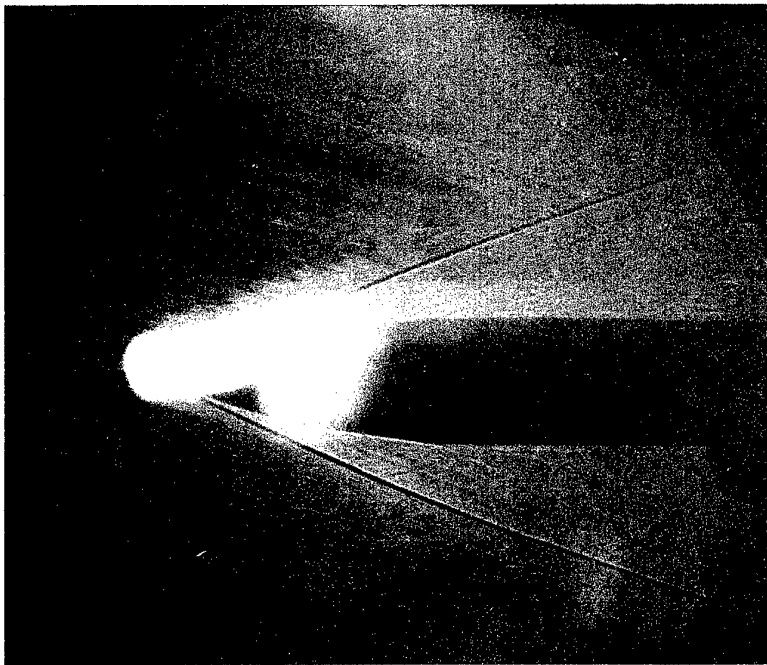
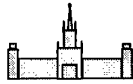
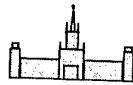


Fig. 2.13. A shadow photo frame of the longitudinal/transversal discharge.



illusion of a diffuse discharge formation in the volume of the airflow (not in a narrow layer near the surface). It could also result in a false conclusion that the shock wave disappears in the plasma region.

Let us briefly consider the effect of the surface discharges on the model's drag in the $M = 4$ airflow. Its more detailed description is to be delivered in the TsAGI's report.

The most considerable drag reduction was observed for flow over the model with spherical frontal part at formation of comparatively stable longitudinal discharges between the spike and the hind electrodes (see fig. 2.11,a). During the discharge period the initial drag coefficient C_x was reduced for 14...15% (i.e. $C_{x1} = 0.85...0.86 C_{x0}$). As the discharge was switched off, C_x grew up very slowly (for several seconds) up to a level C_{x2} that was about 3...4% less than the initial level C_{x0} . It is likely to be a result of plasma modification of the model's surface, that improves its aerodynamic characteristics. It is substantiated by a special experiment with flow over the model with no discharge for about 15 minutes after the plasma aerodynamic experiment. The value of C_x in this experiment was equal to C_{x2} . A qualitative temporary behavior of the drag coefficient at one of the plasma aerodynamic experiments on flow over a model with a discharge is shown on fig. 2.14.

At experiments with conic frontal part of the model a 6...7% drag reduction was observed, that is rather a good result.

It was absolutely unexpected that the value of C_x was also reduced at flow over the models with the ring discharge which was shunting the main interelectrode gap. The effect is however weaker than that at the longitudinal discharges, C_x was reduced for 2.5...4% (in dependence on the discharge input power). It was observed at numerous experiments with both types of models, and was independent on the shape of model's frontal part. It seems rather understandable: the discharge in such cases is formed on the model's lateral surface downstream its frontal part. Drag reduction here may be a result of existence of rather a long plasma region downstream the discharge around the lateral surface, that can shift a coordinate of laminar-turbulent transition, and therefore reduce the viscous friction component of drag.

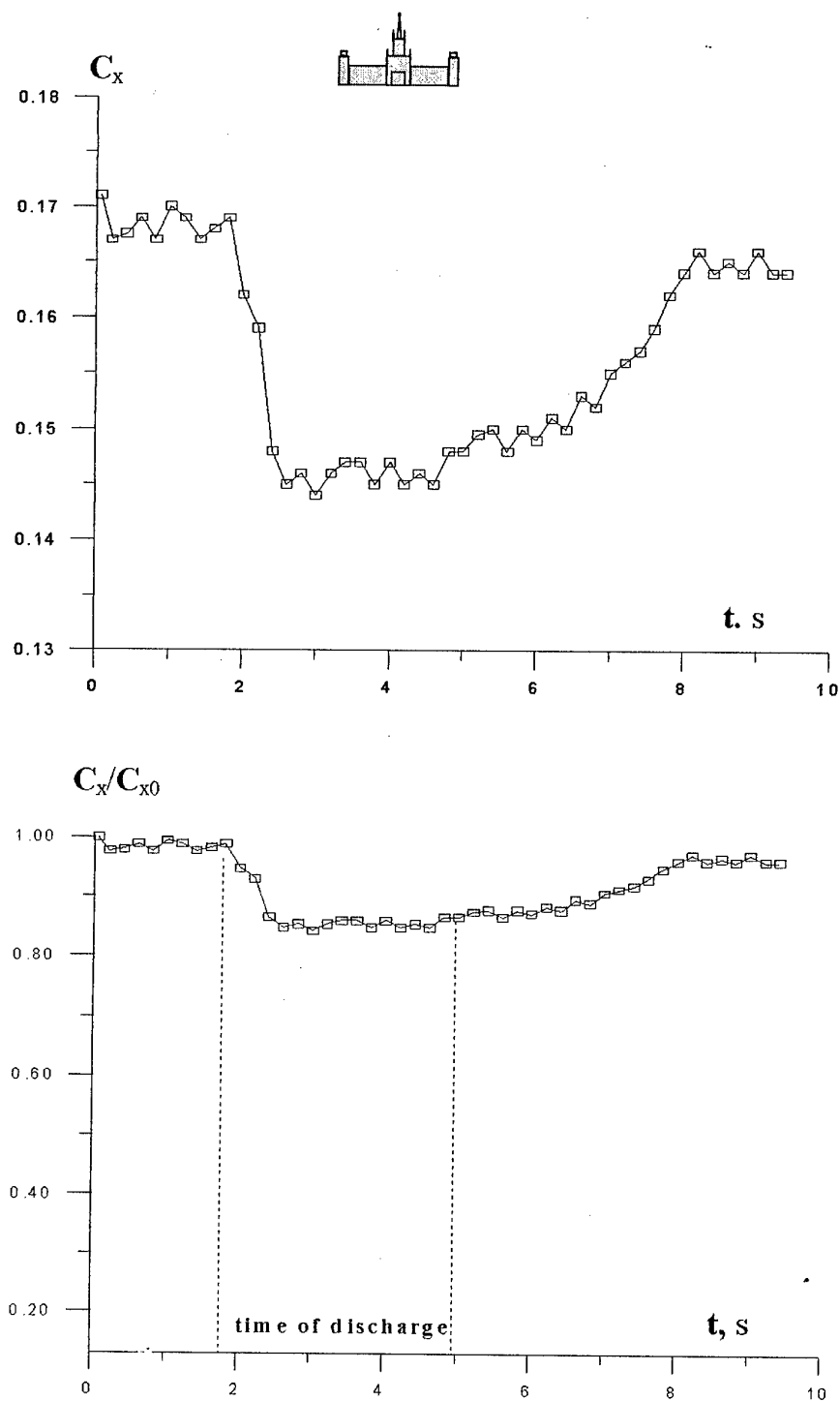
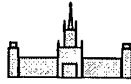


Fig. 2.14. Drag coefficient temporal dependence, the ceramic model with spherical frontal part, AC 4 A, $M = 4$



2.2. Spectral Diagnostics of Plasma Parameters

2.2.1. A Spectroscopic Method of Measurement of Gas Temperature

Information about gas translation temperature T_g is important for study of plasma processes. The simplest possible case for molecular plasma corresponds to local thermodynamic equilibrium, then $T_g = T_V = T_R$, here T_V and T_R are vibration and rotation temperatures, respectively. T_V and T_R are parameters of fitting of population of vibration and rotation energy states of molecules to the Boltzmann function, they characterize distribution function of molecules. Both T_V and T_R can be extracted from plasma radiation spectra.

In non-equilibrium plasmas T_g can be also determined on base of measurement of T_R [57-68]. Spectra of plasma radiation provide information about rotation temperatures T_R^* of molecules in excited electron states. The dependence of T_R^* on intensity of a rotation structure spectral line I_{lk} that corresponds to a transition between l -th and k -th states is given by a formula [57]

$$(k_B/B^*) \ln(I_{lk}/i \nu_{lk}^4) = C - j(j+1)/T_R^*$$

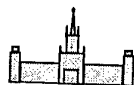
here k_B is the Boltzmann constant, j is a total molecular moment of momentum, i is a quantum mechanical coefficient of intensity, ν_{lk} is the frequency of radiation quantum, C is a constant. One can extract T_R^* by plotting a function $(k_B/B^*) \ln(I_{lk}/i \nu_{lk}^4)$ over $j(j+1)$, and measuring its slope $\text{tg} \alpha$:

$$T_R^* = 1/\text{tg} \alpha.$$

For a stable molecule a possibility of change its rotation energy at excitation is negligible, and rotation distribution functions for excited and basic molecular states are identical, $T_R = T_R^*$. Effective exchange of translation and rotation energies at collisions results in equality of T_g and T_R of molecules in basic electron state.

But at realistic conditions there are some peculiarities that must be paid account to [57].

If molecules take part in plasma chemical reactions, a part of their activation energy can transfer to rotation energy, that results in distortion of initial rotation distribution function, and $T_R \neq T_R^*$. It is especially characteristic to chemically active radicals.



Another source of errors is bound with the fact that spectra yield not T_R but B^*/T_R , here B^* is the rotation constant for upper state at radiation transition. At electron impact excitation of this state, rotation energy distribution can be conserved, but it corresponds to a temperature

$$T_R = T_g B^*/B^o,$$

here B^o is the rotation constant for the basic state.

Thus, stable molecules with $B^* \approx B^o$ should be chosen for measurement of T_g .

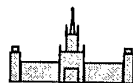
The second positive band of nitrogen is widely used. Here one can take ν_{ik} to be a constant (the corresponding error $\approx 0.5\%$ is negligible), $B^* = 1,826$; the formula for T_R looks like

$$0,89 \ln(I_{ik}/i) = \text{Const} - j(j+1)/T_R.$$

In [68] it is suggested to determine the gas temperature of nitrogen at high pressure on base of unresolved cyan bands with threshold wavelengths 3883 \AA and 3871 \AA . At the present experiments cyan is generated at model erosion. Three ways of temperature measurement are available with use of data presented in [68], these methods are based on: 1) – ratio of integrals of radiation of the two bands; 2) – ratio of threshold intensities of these bands; 3) – distribution of rotation transition intensities of (0;0) band with threshold wavelength 3883 \AA .

2.2.2. A Method of Measurement of Vibration Temperature of a Molecular Plasma

Vibration excitation in a molecular plasma as a rule affects ionization and gas heating [57, 69]. In [69] a method of determination of vibration levels population of nitrogen basic electron state $X^1\Sigma_g^+$ is suggested. It is based on a measurement of radiation intensities in bands of the second positive nitrogen system. Conditions are pointed out, at which the electron state $C^3\pi_u$ is populated due to electron impact excitation of the basic $X^1\Sigma_g^+$ state. De-excitation of vibration levels of the state $C^3\pi_u$ is bound with radiation, because its characteristic time (10^{-7} s) is much less than that of vibration and rotation relaxation and of diffusion.



Let the vibration levels v''_x of the basic nitrogen electron state are distributed according to a function $f(v''_x)$, i.e.

$$n(v''_x) = n_o f(v''_x).$$

Then in case the conditions mentioned above are met, a stationary population of $C^3\pi_u$ vibration levels v'_C is given by

$$n(v'_C) = (n_e n_o / A(v'_C, v'_B)) / \sum_{v''_x} \langle \sigma(v'_C, v''_x) \rangle f(v''_x),$$

here n_o is a number of molecules in $X^1\Sigma_g^+$ state and $v''_x = 0$; $\langle \sigma(v'_C, v''_x) \rangle$ is a mean cross section of excitation of v'_C $C^3\pi_u$ levels, n_e is electron concentration, $A(v'_C, v'_B)$ is a probability of radiation of the second positive nitrogen system, v''_x are vibration quantum numbers of $B^3\pi_g$ state.

As the process of excitation of the $C^3\pi_u$ vibration levels due to electron impact of the basic $X^1\Sigma_g^+$ state is fast in comparison with vibration period, these probabilities can be considered to be in a direct proportion to the Franck-Condon coefficients for the Tanaka system $C^3\pi_u \rightarrow X^1\Sigma_g^+$. Then the previous equation takes form

$$n(v'_C) = C \sum_{v''_x} q(v'_C, v''_x) f(v''_x),$$

here C is a constant independent on v''_x . At computation of the sum one can take only first 5 terms, because the population of the vibration levels is a steep falling function of v . Provided relative populations of the first 5 levels of the $C^3\pi_u$ state are known, one can calculate relative populations v''_x of the basic electron states as a solution of a set of equations

$$n(v'_C) = \alpha \sum_{v''_x=0,1,2,3,4} q(v'_C, v''_x) n(v''_x),$$

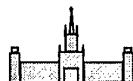
here α is a normalizing coefficient. The relative populations of the $C^3\pi_u$ state levels can be determined experimentally with application of a usual method (on base of relative intensities of bands of the second positive nitrogen system $C^3\pi_u \rightarrow B^3\pi_g$).

Molecular spectroscopy gives the following formula for a radiation intensity of a electron-vibration band:

$$I(v'_C, v''_B) = C' S_e n(v'_C) \nu^4(v'_C, v''_B) q(v'_C, v''_B),$$

here S_e is a strength of electron transition, $q(v'_C, v''_B)$ are the Franck-Condon factors, $\nu(v'_C, v''_B)$ is a frequency of transition, C' is a constant independent on the quantum numbers v'_C and v''_B . After taking logarithm, one can get

$$\ln n(v'_C) = \ln C' + \ln [I(v'_C, v''_B)] / [\nu^4(v'_C, v''_B) q(v'_C, v''_B)],$$



Thus, one can get the relative populations v''_X and the vibration temperature of the nitrogen basic electron state on base of measurement of relative intensities of the electron-vibration bands v'_C .

2.2.3. A Set Up for Spectral Diagnostics

For gas temperature measurement at the plasma aerodynamic, a diagnostic set up has been assembled. Its schematic draft is shown on fig. 2.15. Radiation of the discharge that is formed on the model 5 in airflow 6 generated by the wind tunnel 7, is projected on a spectral device input slot 1, through a window 8, a mirror 4, and a focusing quartz lens 2 (with focal length $f = 25$ cm). The lens diameter and f were chosen so that to provide projection of the discharge's image with reduction $k = 12$, and use of all the light-gathering power of the device. A spectrograph CTЭ-1 was used, its inverse linear dispersion being 0.35 nm/mm for the spectral region of 300...400 nm. Photo film exposition time was 1.5...2 s.

In order to measure the discharge gas temperature spatial distribution, a prism 3 was used that could provide orientation of the discharge image either parallel or normal to the slot. Either axial or radial discharge spectral brightness distribution was registered, which yielded either longitudinal or radial temperature distribution (for fixed radial or axial coordinate).

The measuring system (including the spectrograph CTЭ-1 and the photo film) was calibrated by registration of standard iron arc spectrum (to get a wavelength scale) through a 9-step light reducer (to reveal the linear region of film darkening) on the same photo film together with the tested spectrum.

The photo films were analyzed with use of a microphotometer ИФО-451.

2.2.4. Experimental Results

A characteristic photo fragment of the discharge radiation spectrum for $M = 2.3$ experiments is shown on fig. 2.16. It contains primarily molecular bands of neutral nitrogen second positive system, and molecular nitrogen positive ion first negative system; in some cases there are also observed much weaker molecular bands of CN.

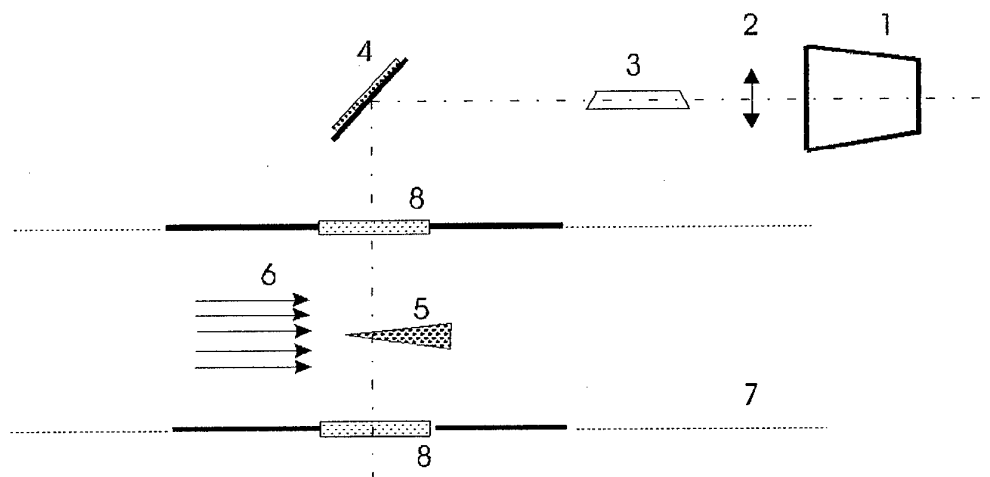
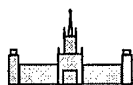


Fig. 2.15. A set up for spectral diagnostics of plasma in airflow: 1 - spectral device input slot, 2 - focusing quartz lens, 3 - prism, 4 - mirror, 5 - model, 6 - airflow, 7 - wind tunnel, 8 - window

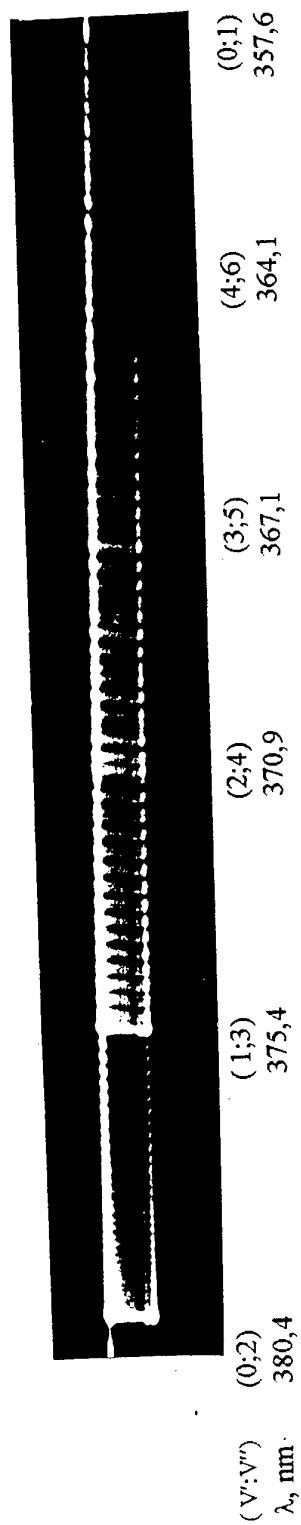
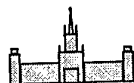
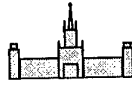


Fig.2.16. A fragment of a discharge at $M \approx 2.3$ air flow radiation spectrum.



An analysis of such spectra shows that the gas temperature at $M = 2.3$ is rather high - $T_g = 1500...2500$ K. Its longitudinal dependence (Fig. 2.17) is not monotonous. Note that its shape does not contradict with computer simulation results (see below).

Fig. 2.18 - 2.20 present spectra (as they look like after processing by the microphotometer ИФО-451) in a wavelength region $\lambda = 360-400$ nm for a $M = 4$ experiment. At experiments with use of ceramic models, their erosion was small (Fig. 2.18), and nitrogen molecular bands prevailed in the spectrum. At acrylic plastic models erosion of surface and electrodes was very strong (Fig. 2.19 - 2.20), and intense CN bands and Cu lines were registered together with the nitrogen spectrum.

The vibration temperature for these conditions ($T_v = 8000...10000$ K) is 3-5 times higher than the gas temperature, i.e. plasma state is very far from equilibrium. A considerable part of plasma energy is accumulated in the vibration reservoir.

In the case of $M = 4$ transversal discharge (between the hind electrodes) the plasma radiation could be registered 2 cm downstream the electrodes. Fig. 2.21 shows the corresponding longitudinal temperature dependencies for discharge current: 1 - 1.1 A, 2 - 1.7 A, 3 - 3.25 A. One can see that the gas temperature grows with current gain, and falls at movement downstream the airflow.

In the case of $M = 4$ longitudinal discharge that took place in a region between the spike and the hind sectioned electrode, this region radiated together with the region 2 cm downstream the hind electrodes. Axial temperature distributions (fig. 2.22) show that in this case the gas temperature also grows with current gain, it holds practically constant in the interelectrode gap, and falls downstream the hind electrodes.

In both cases the vibration temperature achieves $\approx 10,000$ K and falls to $5,000...6,000$ K 1.5 cm downstream the hind electrodes.

Thus, a strong nonequilibrium of translation and vibration temperatures ($T_v/T_g \approx 10$) of the discharge plasma at plasma aerodynamic experiments is observed. It can affect energy balance and all the conditions of supersonic flow over a body.

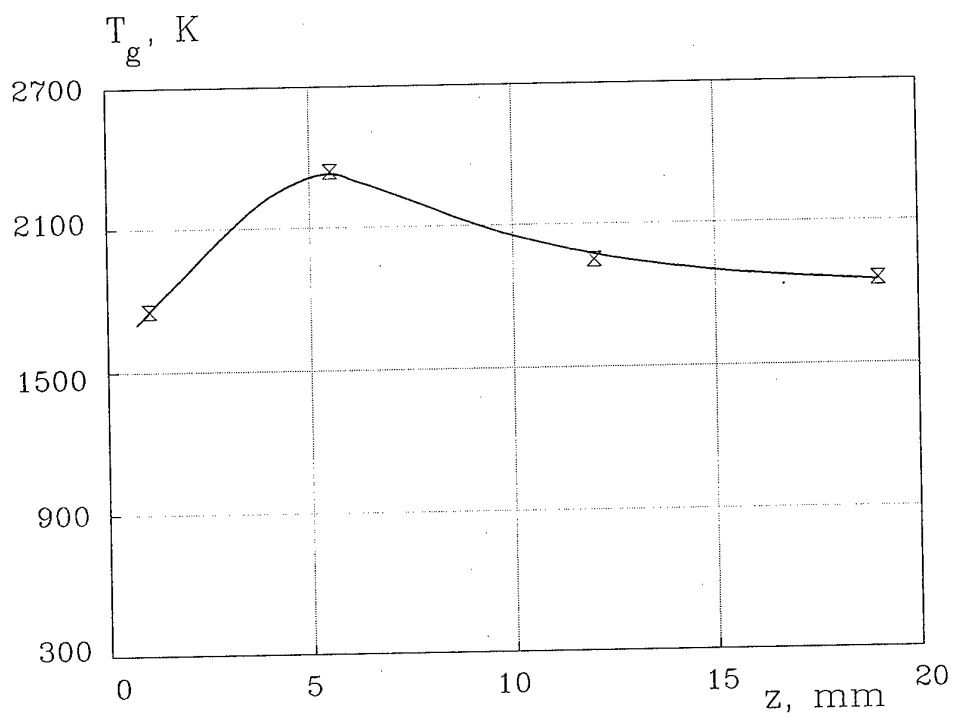
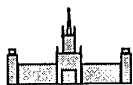


Fig. 2.17. Longitudinal distribution of gas temperature for a model with spherical frontal part at $M = 2.3$ and DC 2 A

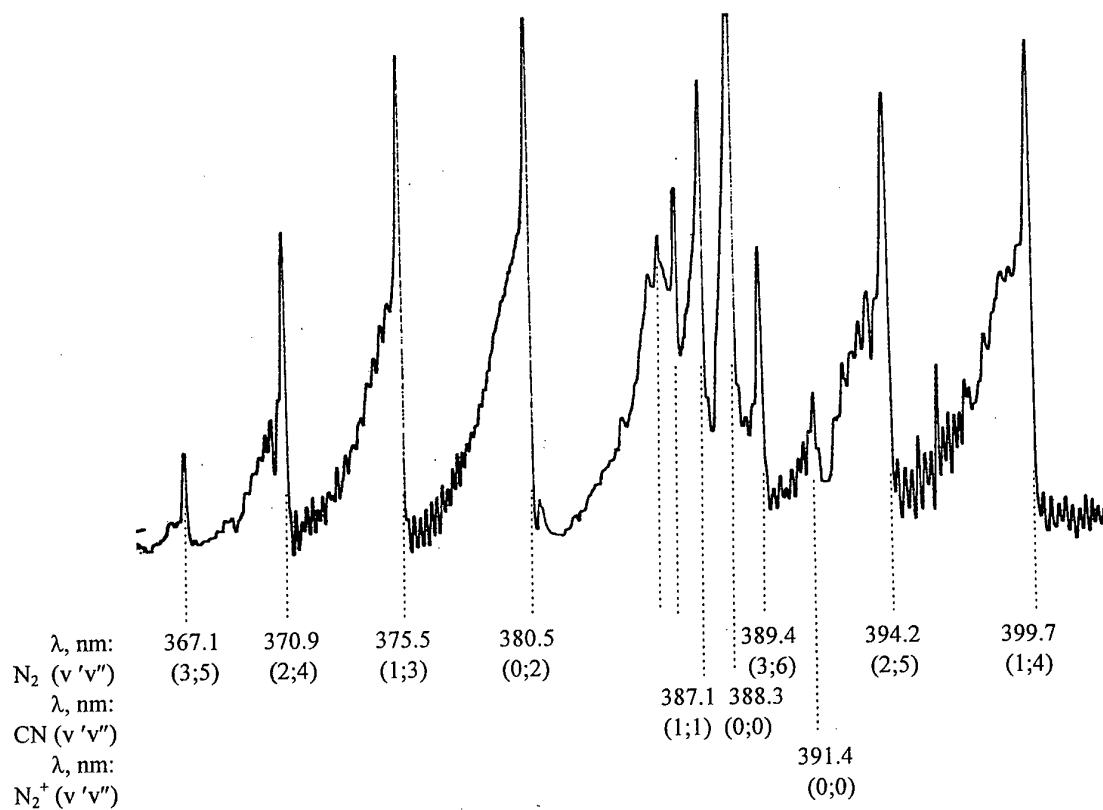
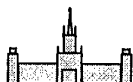


Fig. 2.18. Plasma spectrum for a longitudinal discharge ($I = 1.5$ A) over the model with conic frontal part at a comparatively weak erosion

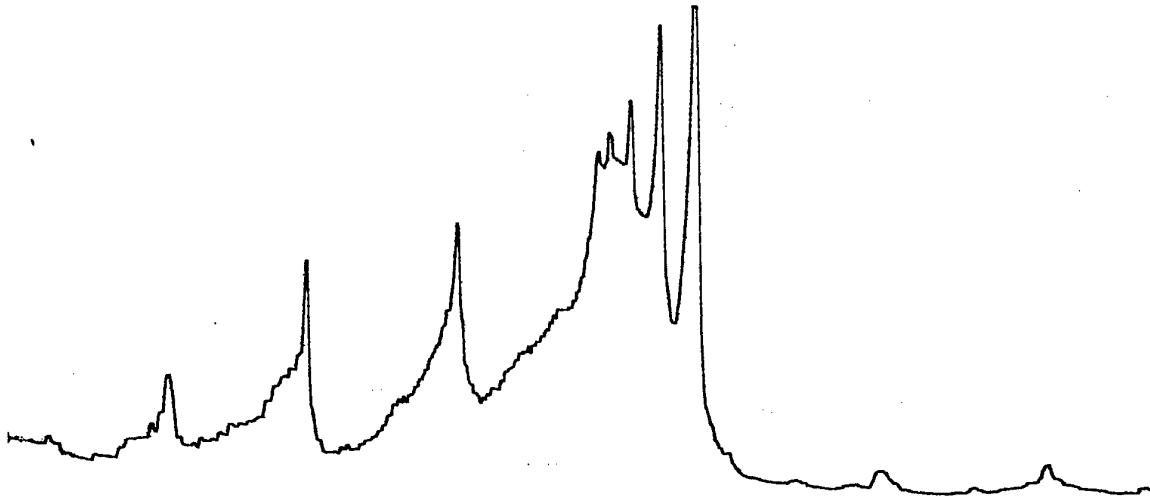
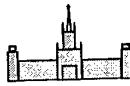


Fig. 2.19. The same region of plasma spectrum as that shown on the previous figure for a longitudinal discharge over the model with conic frontal part at a strong erosion of the model surface

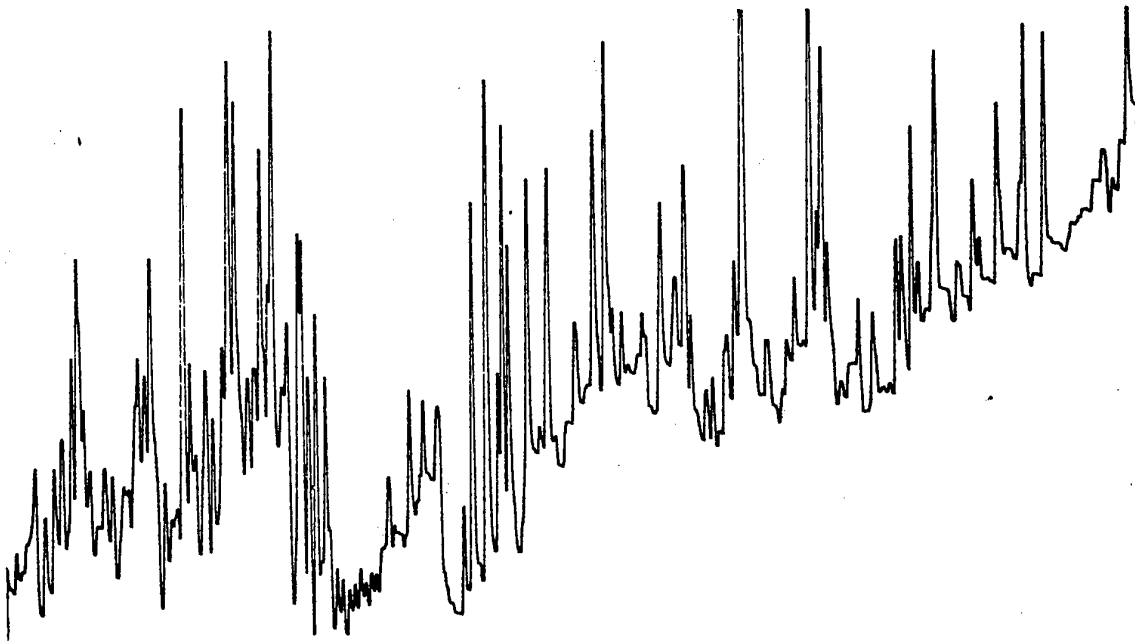


Fig. 2.20. The same region of plasma spectrum for a longitudinal discharge over the model with conic frontal part at a strong erosion of both electrode and model surfaces

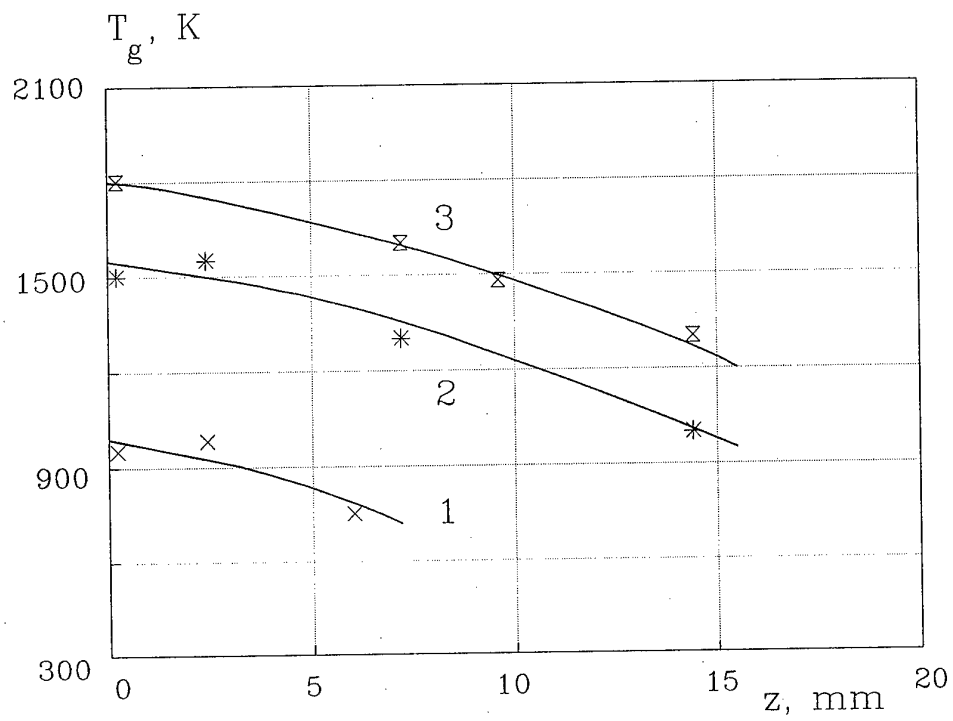
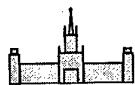


Fig. 2.21. Longitudinal distribution of gas temperature for a transversal discharge over a model with spherical frontal part at $M = 4$:
1 - AC 1.1 A, 2 - 1.7, 3 - 3.25

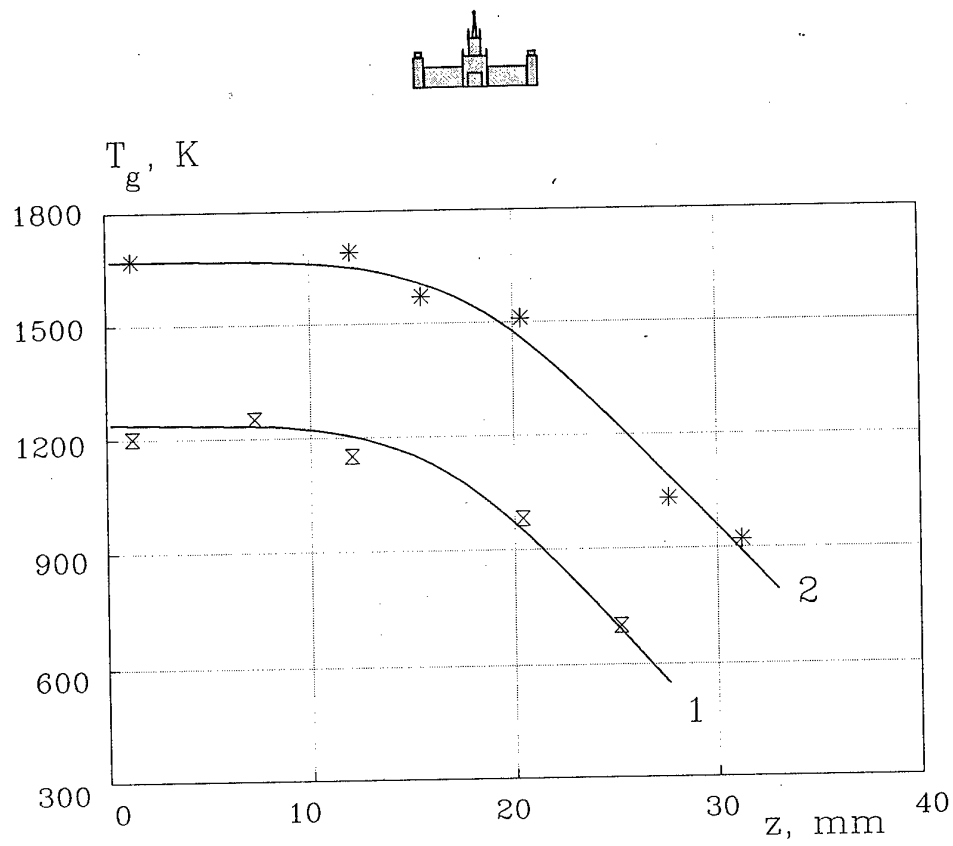
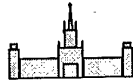


Fig. 2.22. Longitudinal distribution of gas temperature for a longitudinal discharge over the ceramic model with conic frontal part at $M = 4$: 1 - AC 1.5 A, 2 - 2.6



2.3. Probe Plasma Diagnostics

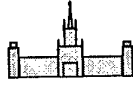
For determination of concentration of charged particles in plasma around the model, the method of double symmetrical probe was used. The sounding electrodes were actually a couple of $\varnothing 1$ mm stainless steel wires, each of them having 10 mm long active part exposed to plasma, and ceramic tube isolation of the rest surface. Our experience of work with probes [51, 55] has shown that stainless steel is one of the best materials for probes to work under such conditions.

The Knudsen number $Kn = \lambda_i/a$ at gas pressure $p > 10$ Torr and gas temperature $T_g \approx 1000$ K is no more than 0.01 (here $2a$ is the probe diameter, and λ_i is a mean free path for ions), i.e. the probe works in the regime of continuous medium.

Note that at considerably greater value of a the plasma region (which is less than 10 mm thick) would be disturbed, at much less a there would be $Kn \sim 1$, i.e. regime of probe would be transient, that would need a detailed numerical simulation for interpretation of experimental data. Moreover, small probe could be quickly burnt down by the plasma flow.

At the parameters of plasma that are of interest for the present plasma aerodynamic experiments, one of the most promoted and reliable probe diagnostic methods is based on analysis of the ionic parts of voltage-current characteristics of a single probe. However another type of probe, double probe, has an important advantage that it does not intercept a considerable part of discharge current, and does not disturb electric current distribution considerably. At sufficiently high probe potential, the ion part of the double probe voltage-current characteristic is close to that of the single probe. That is why for diagnostics of plasma in our region of parameters it is possible to apply for the double probes theories developed for the ion part of voltage-current characteristics of the single probes.

The active sounding surfaces in present experiments were positioned normally in respect to the airflow. It was made so because of the fact that at parallel positioning (as it was often



made before) a considerable disturbance takes place [70], its influence depends strongly on an angle between the surface and the airflow velocity.

To measure the ionic parts of voltage-current characteristics $I_p(V)$, an electric scheme with optical (radiating diode – photosensor) isolation of the probe circuit from the ground connection. A battery of capacitors with low inductance was applied. It was charged by a power source to a necessary voltage, then disconnected from the source, and discharged with a time constant determined by its capacity and a resistance of the boundary layer plasma - sounding electrode surface. Such scheme was chosen in order to prevent ground connection and shortcut after the main discharge ignition either through the power supply source, of through the measurement circuit.

Probe diagnostics deals with complicated phenomena in the boundary layer plasma - sounding electrode surface, and different electric parameters, sounding electrode constructions, and formulae for plasma parameters extraction should be applied for different regions of plasma characteristic parameters.

For preliminary estimates of the present probe regime, a formulae [70]

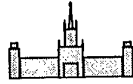
$$j = en_i v_{iw}/4$$

was applied, here v_{iw} is ionic thermal speed at the temperature of the sounding electrode surface. On base of measured current one can get $n_i \approx 10^{14} \text{ cm}^{-3}$, that yields

$$a \gg \lambda_i > r_D$$

(here r_D is the Debye screening distance), i.e. the boundary charge double layer is practically free of collisions. The gas dynamical boundary layer thickness

$$\delta \approx a/\text{Re}^{1/2}, \text{Re} = v a/D.$$



At diffusion coefficient $D \approx 10^2 \text{ cm}^2/\text{s}$, the Reynolds number (that characterizes the airflow influence) $\text{Re} < 10^2$, $\delta \approx 10^{-2} \text{ cm}$, i.e. $\delta \gg \lambda_i$, $\delta \gg r_D$. If one neglects chemical reactions in the gas dynamical boundary layer and collisions in the boundary charge double layer, then asymptotic approximations of boundary layer theory [71,72] yield the following formula for the saturation ion current on the windward part of the cylindrical probe normal to the airflow:

$$j_c = C e n_i (D v / a)^{1/2},$$

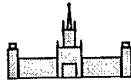
here $C \approx 0.5$ depends weakly on plasma composition and a ratio of electrode and plasma temperatures.

Account of chemical reactions in the gas dynamical boundary layer and collisions in the boundary charge double layer needs complicated numerical calculations. Let's estimate the influence of chemical reactions. If one supposes that basic plasma ion is NO^+ , and the main reaction is its dissociative recombination with rate coefficient $\alpha \approx 5 \cdot 10^{-8}$, the characteristic length of recombination

$$r_{ch} = (2D/\alpha n_i)^{1/2} < \delta,$$

i.e. chemical reactions change the plasma parameters, and should be taken into account. Numerical computations [73] show that the reactions yield a coefficient about 2...3 in the final formula for n_i . Account of collisions results in less amendment.

Electron concentration is about 10^{14} cm^{-3} , this value is between those characteristic for arc and glow discharges.



3. Theoretical Studies of Supersonic Discharge Physics

Major elementary processes in plasma under conditions of the aerodynamic experiment are considered. As a first stage of detailed theoretical research, there have been fulfilled two numerical studies, which consider the phenomenon from different aspects, and are complementary to each other.

3.1. General Consideration

General Approach to Theoretical Investigation

Consider weakly ionized air plasma state under conditions characteristic for studies of plasma applications in aerodynamics with account of all the essential aspects of the phenomena listed above. The corresponding mathematical job definition can be composed of 3 blocks (see Fig. 3.1): - gas dynamics, equations for electromagnetic field, and plasma processes.

The field interacts with the plasma, and plasma interacts with the neutral gas.

The gas discharge plasma in airflow is a very complicated non-equilibrium substance with numerous sorts of neutral and charged particles (different excited states of different types molecules, radicals, ions), its composition depends strongly on its «history», and most of the main parameters cannot be plotted as functions of few arguments (say, F/n_m , T , n_e/n_m , and humidity [24]), as they use to do it for a quasi stationary plasma state of glow discharges in a motionless cold gas. The most important for present applications are the parameters that affect the few output values that are required from the plasma block for work of the blocks of gas dynamics and electromagnetic field.

The set of processes involved (and the corresponding set of equations) is too extensive for immediate computer simulation. The idea of theoretical investigation of the phenomenon is a step-by-step simulation.

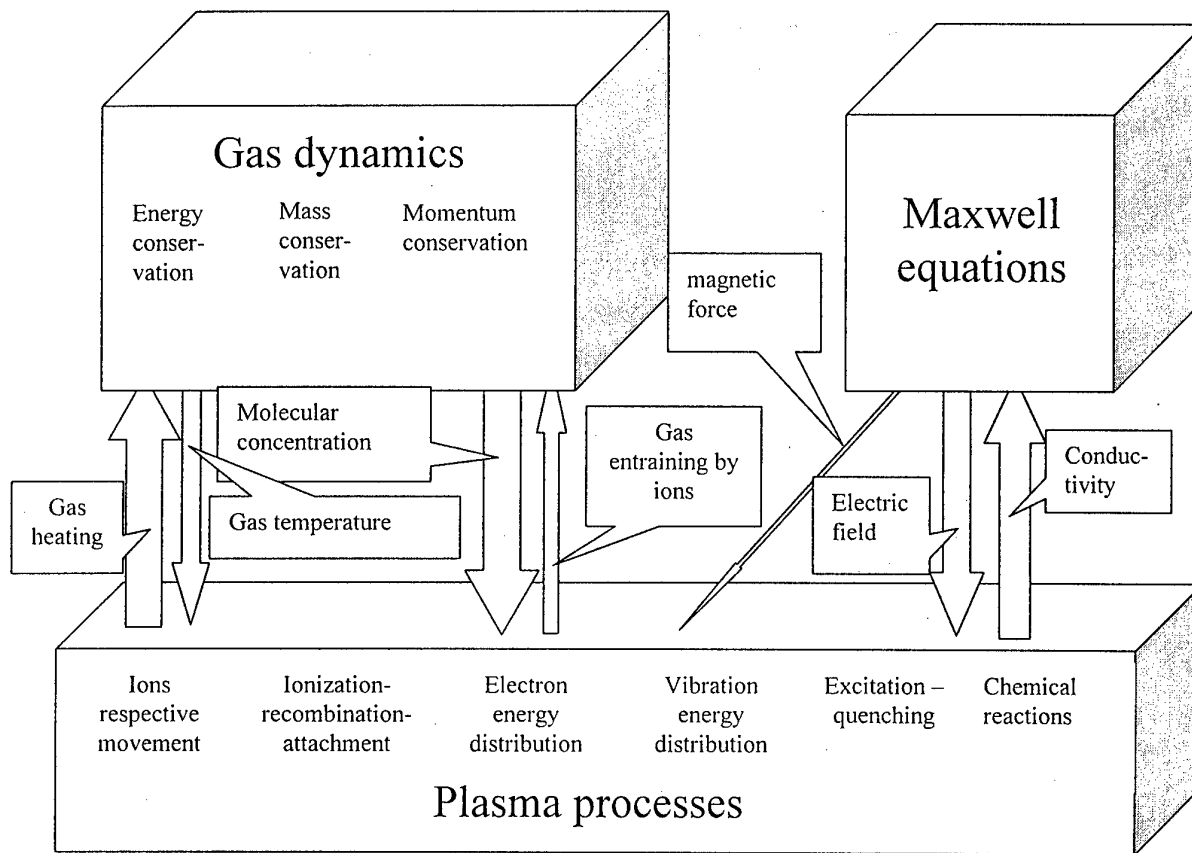
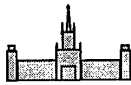
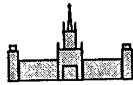


Fig.3.1. On major processes in plasma at the aerodynamic experiments. Three main blocks and information flows

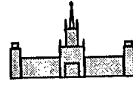


At the first stage (that is implemented in the present work), the whole problem is divided into two different, almost independent approaches, which are based on different mathematical models. One of them considers in details the plasma block (see fig. 3.1), with a radical simplification of the gas dynamic and field aspects. It is based on one-dimensional steady equations, but it takes into account all the details of plasma reactions mentioned above. The other one combines the other two blocks (see fig. 3.1) – traditional gas dynamics and field equations (in non-stationary two-dimensional case), but plasma properties are simplified. Both models are good enough to produce some reliable qualitative results helpful for understanding the phenomenon. Neither of the two approaches is able to describe all the aspects of the phenomenon.

At the second stage (which is desirable to be fulfilled at a continuation of the present work) it is reasonable to combine the two models into one, with use of all the physical and methodical experience of the first stage. This model is to provide a proper quantitative description of the phenomenon in terms of traditional plasma dynamics and plasma chemistry.

A thorough analysis of results of such modeling in comparison with results of detailed experimental study will allow to realize relative roles of different plasma factors, and possibly to extract new, previously unknown effects

At the second stage (which is desirable to be fulfilled at a continuation of the present work) it is reasonable to combine the two models into one, with use of all the physical and methodical experience of the first stage. This model is to provide a proper quantitative description of the phenomenon in terms of traditional plasma dynamics and plasma chemistry. A thorough analysis of its results in comparison with results of detailed experimental study will allow to realize relative roles of different plasma factors, and possibly to extract new, previously unknown effects.



Field and gas dynamic equations

Equations for neutral components:

$$\partial \rho_g / \partial t + \text{div}(\rho_g \mathbf{v}_g) = 0,$$

$$\rho_g d\mathbf{v}_g/dt = -\text{grad} p_g + q + A,$$

$$n_g dE_g/dt = -p_g \text{div} \mathbf{v}_g + S,$$

they differ from the traditional equations of gas dynamics by presence of an effective force A and a nonlinear heating S , which are defined by plasma processes (here n_g , ρ_g , p_g , \mathbf{v}_g , E_g are the gas concentration, density, pressure, velocity, energy of translations and rotations, q is a viscous term, $\rho_g = m_m n_g$, m_m is a molecule mass, $n_g = n_m + 0.5 n_a$). The total gas pressure and energy in case of weak ionization

$$p_g = k_B (n_m + n_a) T_g, \quad E_g = k_B T_g (5/2 n_m + 3/2 n_a) / n_g$$

(k_B is the Boltzmann constant).

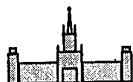
The boundary conditions for these equations can be traditional for flow over a body consideration – e.g., gliding on the walls and the axis, and free entry and exit before and after the body.

To define the electric field \mathbf{F} distribution, one has to solve the Maxwell equations

$$\text{div} \mathbf{F} = e (n_i - n_e) / \epsilon_0, \quad \text{rot} \mathbf{F} = -\partial \mathbf{B} / \partial t,$$

$$\text{rot} \mathbf{B} = \mu_0 \mathbf{j}, \quad \text{div} \mathbf{B} = 0, \quad \mathbf{j} = \sigma \mathbf{F},$$

in quasi steady case ($\partial/\partial t \approx 0$, i.e. with a potential electric field), at the magnetic Reynolds number $\text{Re}_m = \mu_0 e n_e \mu_e v^* l^* \approx 10^{-3}$ being much less than unity; it means that a fact of the plasma conductor movement does not influence the electromagnetic field distribution (σ is conductivity, $\sigma = e n_e \mu_e$, μ_e is electron mobility in the electric field \mathbf{F}).



Plasma processes define spatial distribution of conductivity.

Distribution functions

Distribution functions of neutral particles and ions are practically the Maxwell functions.

This assumption under conditions of interest is not always acceptable for electrons.

Deviations from the equilibrium distribution function can take place due to energy losses of electrons at inelastic collisions, namely, at vibration and electron excitation of molecules. The competing processes that fill the gaps in the distribution function are electron-electron elastic collisions and energy gain from electric field (see fig. 3.2).

The higher is a relative electronic concentration n_e/n_{mol} (i.e. at approach to a boarder between weakly and strongly ionized plasmas), the weaker are the deviations from the Maxwell function. E.g., equilibrium condition for vibration energy band ($\approx 1.5 \dots 3.5$ eV for nitrogen molecules) is

$$E_e \nu_{ee} / (\Delta E_v \nu_{ev}) \gg 1,$$

here ν_{ee} , ν_{ev} are frequencies of electron-electron elastic collisions and e-V excitations, ν_{ee} is proportional to n_e , ν_{ev} is proportional to n_{mol} . This condition can be violated in weakly ionized regions of electric current distribution, its account results in considerable (about decimal order of magnitude) changes of molecular excitation rates. In hot and rarefied regions, however, electron distribution function can be close to the Maxwell function: e.g., at mean electron energy $E_e = 2$ eV, energy exchange at an inelastic collision $\Delta E_v = N_{e-v} \hbar \omega \approx 1$ eV (it corresponds to excitation of about $N_{e-v} = 3$ quanta of N_2 molecular vibrations, $\hbar \omega$ is the vibration quantum, for nitrogen $\hbar \omega = 2330 \text{ cm}^{-1}$), and with respect to the Coulomb e-e cross sections and experimental cross sections for N_2 molecular vibrations excitation, one can get at $T_g \approx 3000 \text{ K}$, $p = 30 \text{ Torr}$:

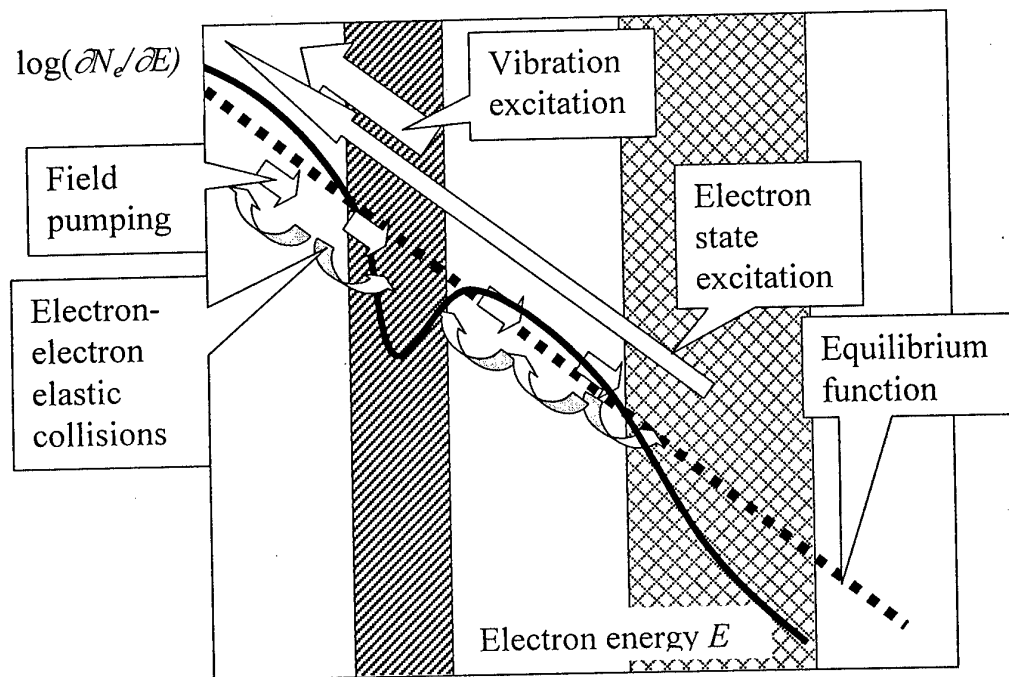
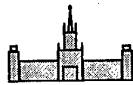
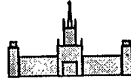


Fig. 3.2. Electron distribution function



$$E_e v_{ee} / (\Delta E_v v_{ev}) = 8 \gg 1.$$

As a result, the number of electrons with energies corresponding to high cross sections of the inelastic collisions is less than at equilibrium, and the number of such collisions is F_I times less. Factors that express the corresponding changes in rates of excitation of vibration and electron states can be estimated as [74]

$$F_I \approx [(1+4C)^{1/2} - 1] / [(1+4C)^{1/2} + 1] / C,$$

here $2C$ is a ratio of frequencies of inelastic and elastic collisions at electron energy E being about T_e higher than the threshold ΔE of the corresponding inelastic process, $E = \Delta E + T_e$. At $C \Rightarrow \infty$ (extremely weakly ionized plasma), $F_I \approx 1/C$, at $C \Rightarrow 0$ (equilibrium), $F_I \approx 1$.

The electron distribution function is determined by a kinetic equation

$$\partial f / \partial t = \delta_F + \delta_{ee} + \delta_{ex} + \delta_{ev},$$

here δ_F , δ_{ee} , δ_{ex} , δ_{ev} correspond to field pumping, electron-electron collisions, excitation of electronic and vibration energy levels, respectively:

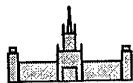
$$\delta_F = 2 / (3 E^{1/2} m_e) (eF)^2 \partial [(E^{3/2} / v_{em}) \partial f / \partial E] / \partial E,$$

$$\begin{aligned} \delta_{ee} &= (2/E^{1/2}) \partial \{ E^{3/2} v_{ee} [f \int_0^E f E^{1/2} dE + (2/3) \partial f / \partial E (\int_0^E f E^{3/2} dE + E^{3/2} \int_E^\infty f dE)] \} / \partial E \approx \\ &\approx (2/E^{1/2}) \partial [E^{3/2} v_{ee} (f + T_e \partial f / \partial E)] / \partial E, \end{aligned}$$

$$\delta_{ex} = \sum_v \sum_l [f(E + E_{vl}) v_{vl}(E + E_{vl}) (1 + E_{vl}/E)^{1/2} - v_{vl}(E) f(E)],$$

$$\delta_{ev} = \sum_v \sum_{v'} [f(E + E_{vv'}) v_{vv'}(E + E_{vv'}) (1 + E_{vv'}/E)^{1/2} - v_{vv'}(E) f(E)].$$

Here E and T_e are electron energy and effective temperature (as a measure of mean energy), v_{em} is a frequency of elastic electron-molecule scattering, summarizing is produced for all the



vibration ν , ν' and electron l energy levels, ν_{vl} and $\nu_{\nu\nu'}$ are frequencies of l -th electron (for transitions with change of electron and possibly vibration quantum numbers) and ν' -th vibration level excitation (for transitions with change of only vibration quantum number), E_{vl} and $E_{\nu\nu'}$ are the corresponding threshold energies.

The electron distribution function remains practically isotropic because of frequent elastic collisions with considerable momentum exchange. It makes it possible to pay account to the deviations of electron distribution function from the Maxwell one only at computation of inelastic collision frequencies, and to consider the plasma as a mixture of continuous media (electrons, ions, molecules, atoms etc.), i.e. in terms of balance for each of the media. The corresponding equations of continuity, momentum and energy conservation are to be written for electrons, ions, atoms and molecules on different excitation levels (see, e.g., [75-76, 57]).

For correct account of vibration excitation, one must consider excitation and quenching of numerous vibration states (or vibration distribution function). But detailed computations show that for the conditions of interest the corresponding nonequilibrium vibration distribution function is close to the Boltzmann function with the corresponding vibration temperature T_V (see, e.g., [57]). So it is possible to assume the Boltzmann distribution for vibrations. T_V is then the only characteristic parameter which defines the extent of vibration excitation.

Plasma composition

Thus, the plasma block contains equations of energy, momentum, and number of particles for gases of electrons, positive and negative ions, and also considers vibration and electron states excitation and other reactions in the neutral components.

There must be considered several equations of plasma chemical kinetics (for balances of atoms, positive and negative ions, vibration and electron states excitation, etc).

If one does not pay a special attention to cathode and anode layers, it is useful to apply quasi neutrality of plasma.



Negative ion balance considers dissociative attachment $K_a = a.n_e n_m$, associative detachment $K_d = d. n_a n_+$, and ion-ion recombination at pair collisions $K_{ii} = \alpha_{++} n_i n_+$ (it results in formation of O atom and highly excited atom instead of positive ion, which will be soon ionized by electron impact):

$$dn_-/dt = K_a - K_{ii} - K_d,$$

here $\alpha_{++} = 0.7 \cdot 10^{-12} (300 \text{ K}/T_i)^{1/2} \text{ m}^3/\text{s}$, $d = 2 \cdot 10^{-16} \text{ m}^3/\text{s}$, a is a function of electron temperature and vibration temperature.

Ionization in the discharge volume may cause considerable growth of number of plasma particles (up to several times in respect to injection from the electrode layers). Its rate is K_I . Dissociative recombination can be also effective: say, for $T_e = 10 \text{ kK}$ for nitrogen its rate $K_{DR}^{N_2} = 3 \cdot 10^{-8} \text{ cm}^3/\text{s}$, and for oxygen - $K_{DR}^{O_2} = 1.5 \cdot 10^{-8} \text{ cm}^3/\text{s}$ ([76]). Recombination due to vibration excitation is less effective (it requires longer periods and cooler gas: at $T_g = 1000 \text{ K}$ its rate is $2 \cdot 10^{-28} \text{ cm}^6/\text{s}^{-1}$, i.e. the characteristic time is several times longer than τ).

Balance of positive ions:

$$\partial n_i / \partial t + \text{div}(n_i \mathbf{v}_i) = K_I - K_{DR}.$$

At the characteristic electron temperatures, molecule dissociation by electronic impact (direct or step by step) can be rather considerable (up to several per cent in gas composition). The inverse processes are as a rule rather slow.

The atomic concentration grows according to an equation

$$dn_a/dt = K_a + K_{ii} + 2(K_D + K_{DR}),$$

here K_D is a total rate of electronic excitations that result in dissociation.



There may be important some reactions of electronically excited metastable nitrogen molecules (see below). Their concentration

$$dn_d/dt = K_{ex} - K_q,$$

here K_{ex} and K_q are the rates of excitation and quenching of the metastable molecules.

Nitrogen vibrations excitation is as a rule very effective. A mean number N_{e-V} of excitations for a N_2 molecule during the characteristic time τ is about a unity or even higher, and the corresponding energy exchange is about $\Delta E_v = N_{e-V} h\omega \approx 0.3 \dots 1$ eV.

If the Boltzmann distribution of vibration excitation is assumed, the vibration temperature T_v can be determined from an equation for a local total number of vibration quanta q_T [76]:

$$dq_T/dt = W_{eV} - W_{VT} - \Pi_\alpha,$$

here $q_T = \sum V n_V \cong n_m / [\exp(h\omega/T_v) - 1]$, n_V is a number of molecules on V -th vibration level, T_v is the vibration temperature, W_{eV} is the frequency of pumping due to e-V excitation processes. For nitrogen it can be calculated as [76]

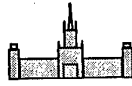
$$W_{eV} \cong n_e n_m P_{01} \{ \exp(-h\omega/T_e) / [1 - \exp(-h\omega/T_e)]^2 - \exp(-h\omega/T_v) / [1 - \exp(-h\omega/T_v)]^2 \},$$

here P_{10} is the first level excitation possibility (see [75,76]). W_{VT} is the frequency of VT quenching.

The processes of V-V excitation and V-T transfer at high ($V \gg \alpha$) vibration excitation levels are taken into account in the term

$$\Pi_\alpha = (4bQ/\Delta^3) n_0^2 \alpha^2 \exp(-2b\alpha^2 - 1), \quad \alpha = T_g/(2xT_v) + 0.5,$$

here $b = xh\omega/T_g$, n_0 can be calculated from normalization



$$\sum n_V = n_m, \quad n_V = n_0 \exp(-2b\alpha V + bV^2),$$

here the summation is performed at least from $V=1$ to $V=\alpha$. An initial condition for the differential equation for T_V calculation corresponds to initial value of element of mass temperature: $T_{V0} = T_V(t=0) = T_{g0} = 300$ K.

Energy flows

There should be taken into account several energy reservoirs in plasma, and a number of processes that cause energy flows between them (see fig.3.3).

Energy of the electric field F passes primarily to electrons, and a smaller part passes to ions.

From electrons, energy passes primarily to vibration reservoir V (at lower fields), and to electron states excitation ex (at higher fields).

Energy is also absorbed by rotations R , molecules dissociation D , and ionization I .

At numerous processes energy leaks to the neutral gas translation energy T .

Electron temperature is the highest ($\sim 10\,000$ K), vibration and excitation reservoirs energies (as well as D , I) correspond to lower temperatures (~ 1000 - $10\,000$ K). The temperatures of ions, T and R reservoirs are the least (~ 100 - 1000 K).

Heavy particles (ions, atoms, and molecules) have practically the same local temperature $T = T_g$, for their characteristic number of elastic collisions is $(v_n/v^*) (l^*/l) \approx 10^4 \gg 1$, and the energy exchange at one collision is about the particle mean kinetic energy (here $v_n = (2T_g/m_n)^{1/2}$ is a thermal velocity of neutral particles with mass m_n). Their rotational temperatures are also practically equal to T_g . Ions are accelerated by electric field between the collisions, their mean energy can deviate from T_g , but the difference is as a rule negligible.

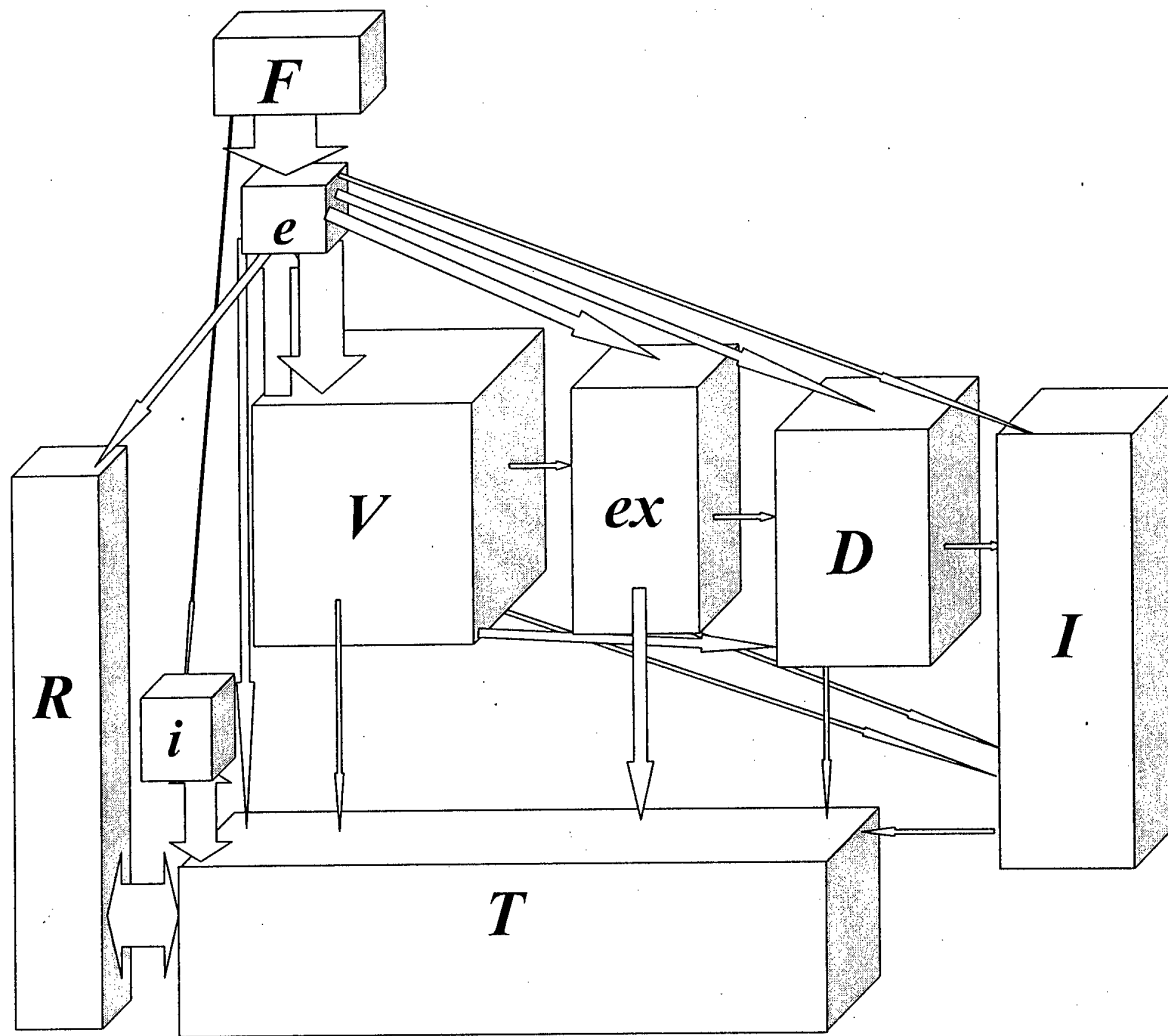
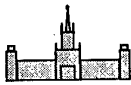
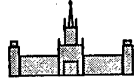


Fig. 3.3. Main energy reservoirs and energy flows



Thus, translation and rotation energy balances of all the heavy particles can be described by one equation.

The electron temperature T_e is as a rule much higher than T_g . At characteristic number of collisions with electrons for a molecule, during the characteristic time τ , being about 10-100, and the energy exchange magnitude $2T_e m_e / m_m \approx 10^{-4}$, possible heating of the gas due to elastic collisions is very small (about 30...100 K only). However in a molecular gas there are several other ways of heat transfer from the electrons. The energy flows that result in gas heating are the following (see fig. 3.4).

Electric field energy input

$$S_F = \sigma F^2, \quad \sigma = en_e \mu_e,$$

μ_e is electron mobility:

$$\mu_e = e / (v_{el} m_e), \quad v_{el} = \sigma_{el} v_{eT} n_m + \sigma_{ee} v_{eT} n_e + \sigma_{ei} v_{eT} n_i,$$

here σ_{el} is a cross section of electronic elastic scattering on the molecules (see [75]), $v_{eT} = (2T_e/m_e)^{1/2}$, σ_{ee} and σ_{ei} are the Coulomb cross sections for scattering on electrons and ions,

$$\sigma_{ee} = 16 \pi a_0^2 (27.2/(2T_e))^2 \ln \Lambda_e, \quad \ln \Lambda_e = 23 + 1.5 \ln(T_e) - 0.5 \ln n_e,$$

$$\sigma_{ei} = \sigma_{ee} / 2^{1/2},$$

here $a_0 = 0.0529$ nm, T_e in eV, n_e in cm^{-3} .

Powers of dissociation and ionization

$$S_D = \Delta E_D K_D, \quad S_I = \Delta E_I K_I,$$

here ΔE_D , ΔE_I are mean amounts of energy needed for one act of dissociation or ionization.

Powers of heating the gas as a result of acceleration of atoms at the process of dissociation after electron impact excitation or dissociative recombination

$$S_{DT} = \Delta E^{ex}_D K_D, \quad S_{RT} = \Delta E^{ex}_R K_R,$$

here ΔE^{ex}_D is an energy of unstable excited molecule before dissociation, which is mean for the states that result from electron impact excitation, and ΔE^{ex}_R is the energy of unstable

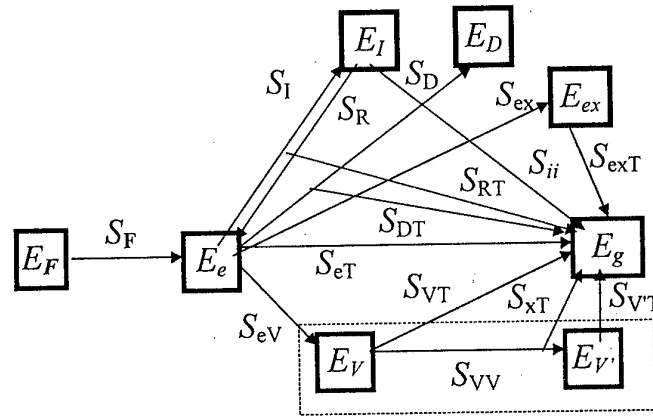
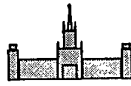
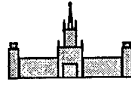
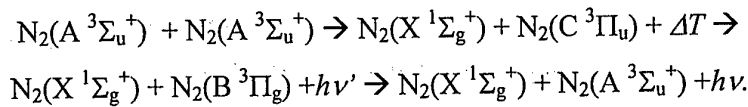
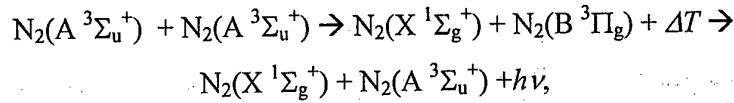


Fig. 3.4. Energy flows that result in gas heating
 E_F - electric energy source, E_e - electron gas, E_{ex} , E_D , E_I - energy of electron excitation, dissociation and ionization, E_V , $E_{V'}$ - lower and upper levels vibration excitation energy, E_g - energy of gas translations and rotations



excited molecule before dissociation which is mean for the states that result from dissociative recombination.

Power S_{exT} of gas heating at electronic metastable excited states quenching due to reaction chains including re-distribution of excitation energy and radiation:



Power of gas heating at recombination of negative and positive ions S_{ii} is determined by recombination rate and the characteristic energy release at collisions during their approach:

$$S_{ii} = n_i k_{ii} \Delta E_{ii}.$$

Power of e-T heating at elastic collisions

$$S_{eT} = (2T_e m_e / m_m) (\sigma_{el} n_e v_{eT} n_m + \sigma_{ei} v_{eT} n_e) n_e.$$

Power of vibration excitation

$$S_{eV} = W_{eV} h\omega.$$

Power of gas heating due to lower vibration levels quenching

$$S_{VT} = W_{VT} h\omega.$$

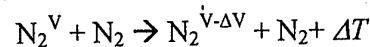
The gas heating power due to VV exchange collisions

$$S_{xT} = \sum_V n_V \sum_{V'} x h\omega (V-V') Q(V+1, V|V', V+1).$$

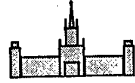
Power of gas heating due to higher vibration levels quenching

$$S_{VV} \cong S_{VT} = I\alpha (h\omega - \alpha x h\omega).$$

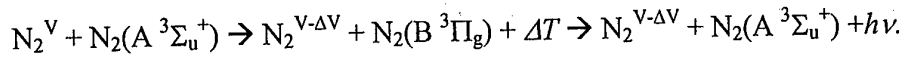
A considerable amount of energy input is stored in the vibration reservoir. Consider the ways of vibration energy conversion to the gas heating in more details. Direct transfer of the vibration energy to the N_2 gas temperature



is very slow. However, if some amount of O atoms is present, then the speed of the gas heating becomes much higher (due to reactions of N_2O formation, internal VV redistribution,



and the oxide molecules dissociation). Still higher heating rates might result from collisions of molecules on high vibration levels N_2^V with metastable excited molecules $N_2(A^3\Sigma_u^+)$; there takes place a transfer of vibration energy to further excitation of the metastable molecules and to the translation energy ΔT , with sequent radiation and formation of the metastable states:



Another channel of vibrations de-excitation is bound up with VV exchange at nitrogen excited molecules collisions, and highly excited molecules generation. This process rate can be calculated with use of an approximation

$$Q(k+1, l|k, l+1) \cong Q^*(l+1)(k+1) \exp(-\Delta(l-k)),$$

here for nitrogen $Q^* \cong 5.10 \cdot 10^{-13} \text{ cm}^3/\text{s}$, $\Delta \cong 0.4$, $k+1, l$ are initial, and $k, l+1$ are final vibration levels of the colliding molecules K and L . At the characteristic excited molecules concentration being about $n_m \approx 0.5 \cdot 10^{18} \text{ cm}^{-3}$ at $l=4$, $k=3$, one can get $Q \cong 50$. At any collision of such a type, a certain amount of energy $x\hbar\omega$ is transferred from vibration to the translation degrees of freedom, for nitrogen $x\hbar\omega = 14.5 \text{ cm}^{-1}$. The total heating during τ due to this mechanism might be considerable.

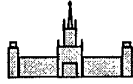
The total nonlinear plasma heating of the gas

$$S = S_{exT} + S_{VT} + S_{VT} + S_{xT} + S_{DT} + S_{RT} + S_{ii} + S_{eT}.$$

Plasma dynamics

Movement of excited and unexcited molecules and atoms can be described by one common equation of momentum conservation, because of effective momentum exchange.

But ions and especially electrons are accelerated by the electric field between the collisions with neutrals, and ion and electron liquids can move quickly in respect to the neutral gas.



One can neglect the processes of neutrals diffusion, for their characteristic time magnitudes are much longer than the characteristic transit time $\tau = l^*/v$. The ambipolar diffusion of electrons and ions is however much more effective than diffusion of neutrals, because its coefficient D_a is about $(1+T_e/T_g) \gg 1$ times higher (here T_e is an effective temperature of electrons). The process might be important in some cases near borders of electric current distribution.

The ion gas velocity is defined with respect to drift of ions in the electric field (associated with frequent elastic scattering on ions and neutral particles which result in a complete momentum loss and relatively small energy exchange), and to the ambipolar diffusion (coupled with the so-called thermal diffusion):

$$\mathbf{v}_i = \mathbf{v}_g + \mu_i \mathbf{F} - \mathbf{grad} (D_a n_e),$$

here μ_i is the ion mobility:

$$\mu_i = e/(v_i m_m), \quad v_i = v_{iT} / l_i, \quad l_i = 1/(n_i \sigma_{ii} + n_m \sigma_{im}), \quad v_{iT} = (2k_B T_g / m_m)^{1/2},$$

here σ_{ii} is the Coulomb cross section for scattering of ions on ions,

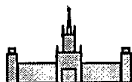
$$\sigma_{ii} = 16 \pi a_0^2 (27.2/(2T_g))^2 \ln \Lambda_i, \quad \ln \Lambda_i = 23 + 1.5 \ln (T_g) - 0.5 \ln n_i,$$

here $a_0 = 0.0529$ nm, T_e in eV, n_e in cm^{-3} , σ_{im} is ion-molecule effective elastic scattering cross section, it is calculated as a sum of a real elastic scattering cross section and a cross section of charge exchange ([75]). D_a is the ambipolar diffusion coefficient,

$$D_a = (l_i v_i / 3) (1 + T_e / T_g).$$

Negative ions drift in the opposite direction relatively the positive ions with approximately the same speed,

$$\mathbf{v}_- = \mathbf{v}_g - \mu_i \mathbf{F} + \mathbf{grad} (D_a n_e).$$



Our estimates have shown that all the traditional forces of ion-molecule interaction (ponderomotive force, gas entraining by the ion drift, etc.) seem to be too small for the conditions of aerodynamic experiments, and one can probably neglect the term A .

One of typical errors of beginners in plasma analysis is to use the «most natural» way of computation of electric field from the Poisson equation, and to calculate charge density n_q as a difference between the concentrations of positive and negative particles. The Poisson equation is useful for analysis of regions with characteristic size being not very great in comparison with the Debye radius (e.g., electrode layers, a microscopic – few microns – vicinity of shock wave front, etc). At modeling of plasma volumes with electron concentration typical for aerodynamic experiments, tremendous computational problems arise: the Poisson equation defines very fast plasma oscillations that demand intolerable time step limitations, and n_q is several orders of magnitude less than n_e , which requires impossible accuracy of numerical computation for n_e , n_i , n_- . The solution of the problem is rather simple: the Poisson equation is unnecessary for computation of all the parameters in plasma (but n_q) and should be expunged from the job definition. The electronic concentration n_e plus concentration of negative ions n_- should be taken equal to n_i (quasi neutrality of plasma).

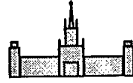
Temperature of electrons is defined by equation

$$n_e dE_e/dt = -p_e \operatorname{div} \mathbf{v}_e - \operatorname{div} \lambda_e \operatorname{grad} T_e + S_F - S_D - S_I + S_R - S_{eT} - S_{ex} - S_{eV},$$

here E_e is electron kinetic energy ($E_e = 1.5 T_e$), the electron gas heat conductivity $\lambda_e = 2.5 T_e n_e / (m_e v_{el})$,

3.2. Simulation of Plasma Kinetic Processes

In [77] a model of the phenomenon was suggested which describes primarily the plasma block (see fig. 3.1), with a detailed account of all the listed reactions of vibration and electron states excitation and quenching, ionization and recombination, attachment, dissociation, non-equilibrium electron distribution function, drift of positive and negative ions, various ways of gas heating, etc.



In order to expedite the investigation, in this model the gas dynamic and field blocks have been simplified according to the following.

There is considered a longitudinal discharge, which forms a plasma channel along a supersonic airflow. It is supposed that gas longitudinal speeds inside and outside the channel are close to each other and to the speed of the unperturbed airflow v_∞ :

$$v_g = v_\infty.$$

It is also quite natural to suppose that the weakly ionized plasma static pressure equals to that of the unperturbed airflow p_∞ , thus gas concentration in the plasma channel

$$n_g = p_\infty / (k_B T_g).$$

It altogether substitutes the gas dynamic block for studies of plasma parameters distribution along the axis, provided the gas temperature T_g is known from simulation of plasma kinetics.

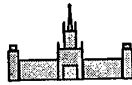
Electric current distribution across the channel is known to be close to Π -shape as a rule. If the current channel cross section A and total current $I = jA$ are known, say, from experimental data, and the plasma conductivity σ is calculated on base of the plasma block, then electric field distribution along the channel can be also obtained as

$$F = j/\sigma.$$

Thus, the field block is also simplified radically.

A steady one-dimensional approximation is used to describe processes in the weakly ionized plasma near the channel axis. Main equations of the model include balances of:
gas temperature

$$\partial T_g / \partial z = (2/7) S T_g / (p_\infty v_\infty),$$



electron mean energy

$$S_F = S_I - S_R + S_D + S_{ex} + S_{eV},$$

vibration quanta

$$\partial q_T / \partial z = (W_{eV} - W_{VT} - \Pi_\alpha - (q_T / n_g) \Delta_r) / v_\infty,$$

(here the term $\Delta_r = v_\infty p_\infty / (k_B T_g^2) \partial T_g / \partial z$ results from radial expansion at heating);
positive and negative ions,

$$\partial(n_i v_i) / \partial z = K_I - K_{DR} - (n_i / n_g) \Delta_r,$$

$$\partial(n.v.) / \partial z = K_a - K_{ii} - K_d - (n./n_g) \Delta_r,$$

neutral atoms

$$\partial n_a / \partial z = [K_a + K_{ii} + 2(K_D + K_{DR}) - (n_a / n_g) \Delta_r] / v_\infty,$$

electronically excited molecules

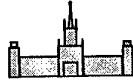
$$\partial n_{ex} / \partial z = [K_{ex} - K_q - (n_{ex} / n_g) \Delta_r] / v_\infty,$$

dynamics of positive and negative ions,

$$v_i = v_\infty + F\mu_i, \quad v_- = v_\infty - F\mu_i,$$

stationary kinetic equation for a local electron distribution function

$$\delta_F + \delta_{ee} + \delta_{eV} + \delta_{ex} = 0$$



with the approximate description of δ_{ee} , and with account of excitation from basic state. The electron distribution function was used at spectral integration of cross sections for calculation of local reaction rates.

The following boundary conditions were applied. Ion concentration at $z = 0$ point (near the frontal electrode) $n_i(z=0) = n_{i0}$, $n_{i0} > 0$ is small in comparison with a characteristic value of plasma concentration n_I' (results do not depend on n_{i0} because of very fast growth of n_i value, and its further stabilization at $z \approx 0$ on the same level n_I'). The rest boundary conditions are quite apparent:

$$T_g(z=0) = T_\infty, q_T(z=0) = n_a(z=0) = n_e(z=0) = n_{ex}(z=0) = 0.$$

The listed above set of implicit algebraic and ordinary differential equations was solved numerically with use of the Newton and the Runge-Kutta methods. Spatial intervals at the vicinity of $z = 0$ point were 30...300 times smaller than a couple of millimeters below (to provide calculation stability at extremely fast alteration of most of the variables). For calculation of electron distribution function f in spatial point z_i , there were used the parameters in the previous point z_{i-1} .

Instead of kinetic equation, in a part of calculations the approximate equations for F_I (see above) have been also used; it did not result in a considerable deviation of magnitudes of the main plasma parameters, and it did not affect qualitative results at all, but a considerable acceleration of computations was observed.

In [77] there has been produced a comparison of computer simulation and experimental results for a longitudinal gas discharge with a geometry which provided a practically free plasma channel, with absence of its contact with the body on its major part (see fig. 3.5), instead of a flow over a body with a complicated shape. The experiments in a wind tunnel at $I = 1.5$ A, $M = 6$, $T_\infty = 36$ K, $p_\infty = 30$ Torr, current channel length $L = 40$ mm, and diameter $2R = 2.5...3$ mm were taken.

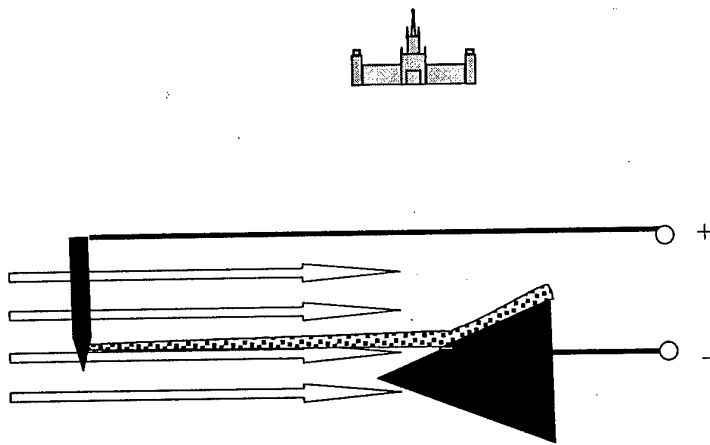


Fig. 3.5. A free longitudinal discharge [ColPr]

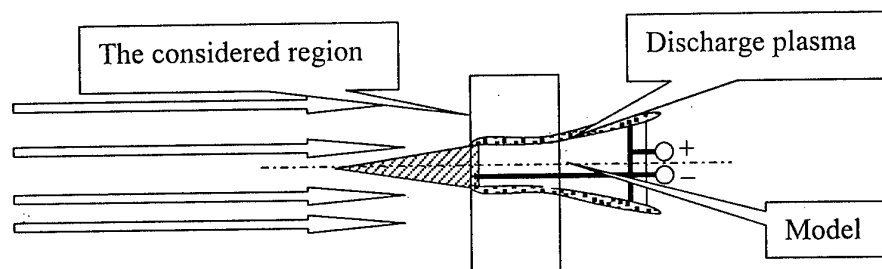


Fig. 3.6. A discharge with flow over a model



At computation these experimental data for I , T_∞ , p_∞ , R , L were used as initial conditions. The model thus contained no degrees of freedom for fitting. A reasonable agreement has been obtained in gas temperature ($\cong 20\ldots 30\%$) and total discharge voltage (experimental voltage is about 30-50% higher, but it includes electrode layers, which have not been taken into account at present computer simulation).

In the present work the similar model has been used for conditions of a plasma aerodynamic experiment with flow over a model (fig. 3.6). A 6 mm long region of one-dimensional cylindrical part of the discharge was analyzed (around the cylindrical spike, between the hind end of the frontal electrode and the forehead of the model). The regime corresponded to that examined at the experiments with the Dr. Klimov's installation ($M = 2.3$, $T = 160$ K, $p = 70$ Torr). According to the experimental data, that exhibit illumination of a boundary layer near the model's surface, a small cross section A of the discharge was taken. but contrary to the previous case, we could not extract the value of A with a sufficient accuracy; it was actually a fitting parameter; we obtained it from a condition of accord between measured and calculated gas temperature. The calculated voltage could not be compared with the experimental one because only a fraction of discharge column was modeled. All the hopes on reliability are based on the fact that the same model did not contradict with experiments for $M = 6$ case (see above). Some results are presented on figures 3.7...3.15.

As it follows from plasma aerodynamic calculation (see below), some of assumptions of this model have proved to be incorrect (e.g. that the speed of plasma flow is equal to the speed of airflow, and plasma pressure is equal to p_∞). But one can still extract the following reliable results.

The results for $M=2.3$ are qualitatively similar to those for $M = 6$, but in the latter case most of parameters change more dramatically.

One can see that there are two different regions in the discharge column (see Table 1). One of them is situated near the frontal electrode, it is considerably short (~ 2 mm long), but most events (electric energy absorption, ionization, vibration excitation, metastable molecules generation, gas heating, etc.) take place primarily there. Another region occupies the rest

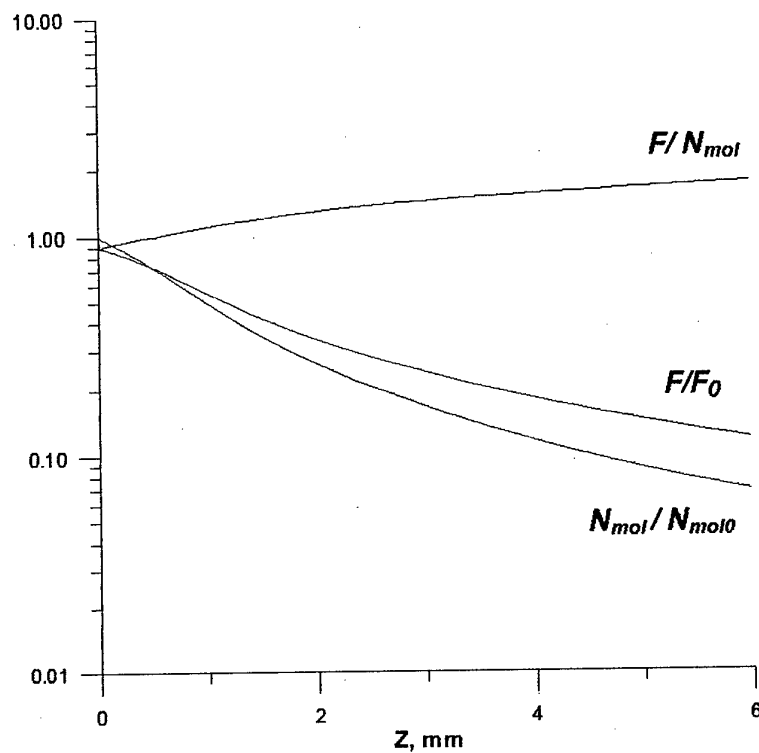
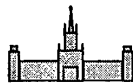


Fig. 3.7. Relative changes of electric field F/F_0 , gas concentration (N_{mol}/N_{mol0}), and the similarity parameter ($\sim F/N_{mol}$), at $T = 160$ K, $p = 70$ Torr

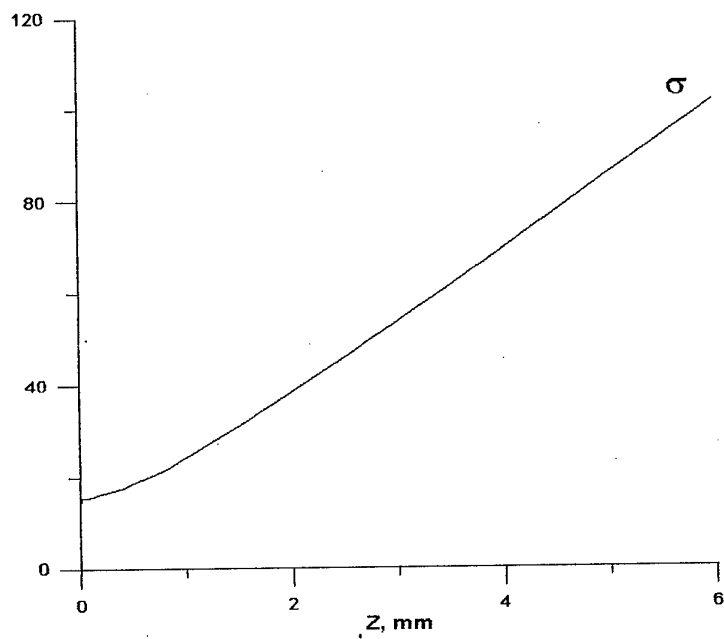


Fig. 3.8. Spatial distribution of plasma conductivity, $1/(\text{Ohm.m})$, at $T = 160$ K, $p = 70$ Torr

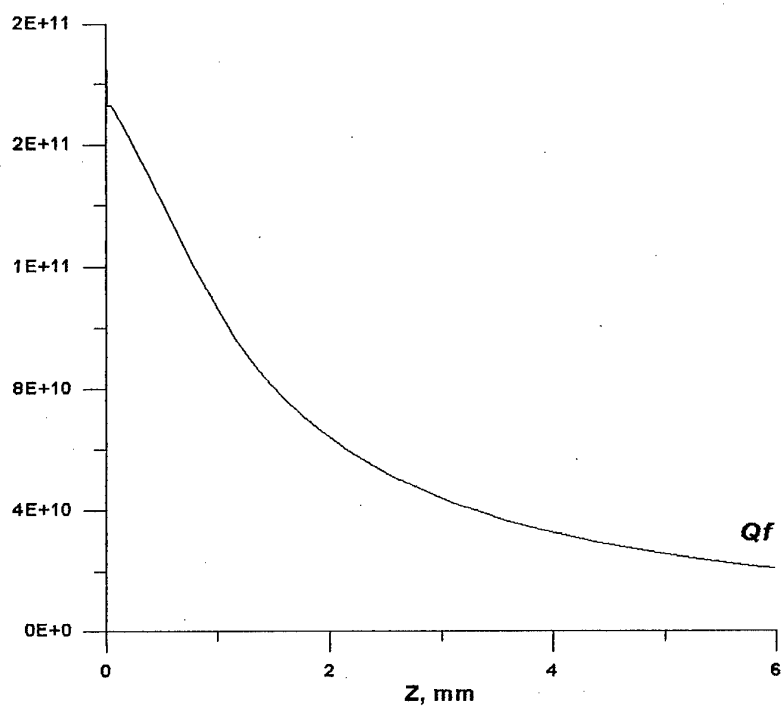
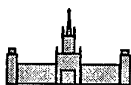


Fig. 3.9. Specific power of Joule heating, W/m^3 , at $T = 160 \text{ K}$, $p = 70 \text{ Torr}$

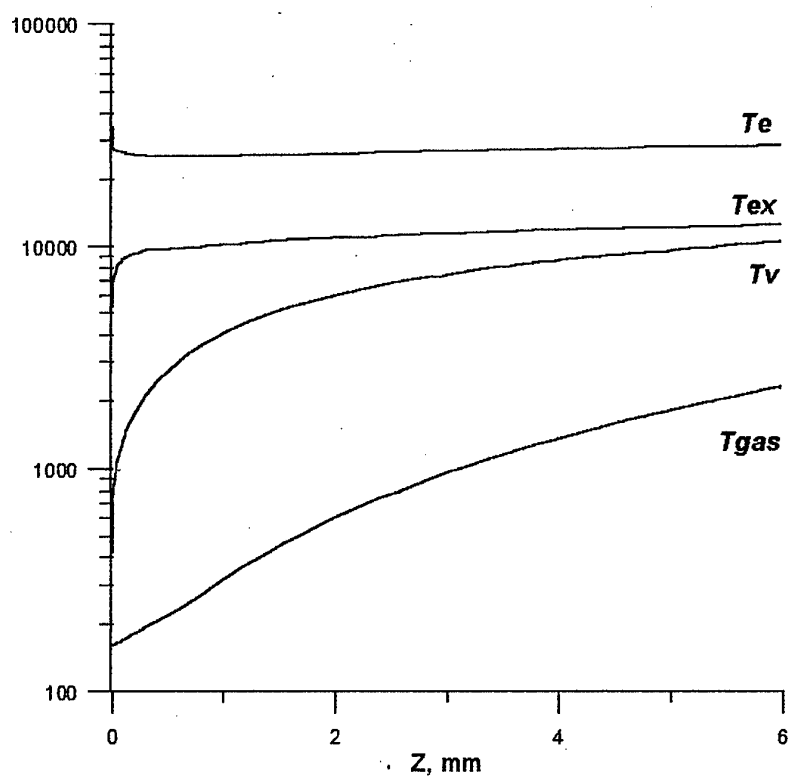


Fig. 3.10. Spatial distributions of plasma temperatures, K, at $T = 160 \text{ K}$, $p = 70 \text{ Torr}$

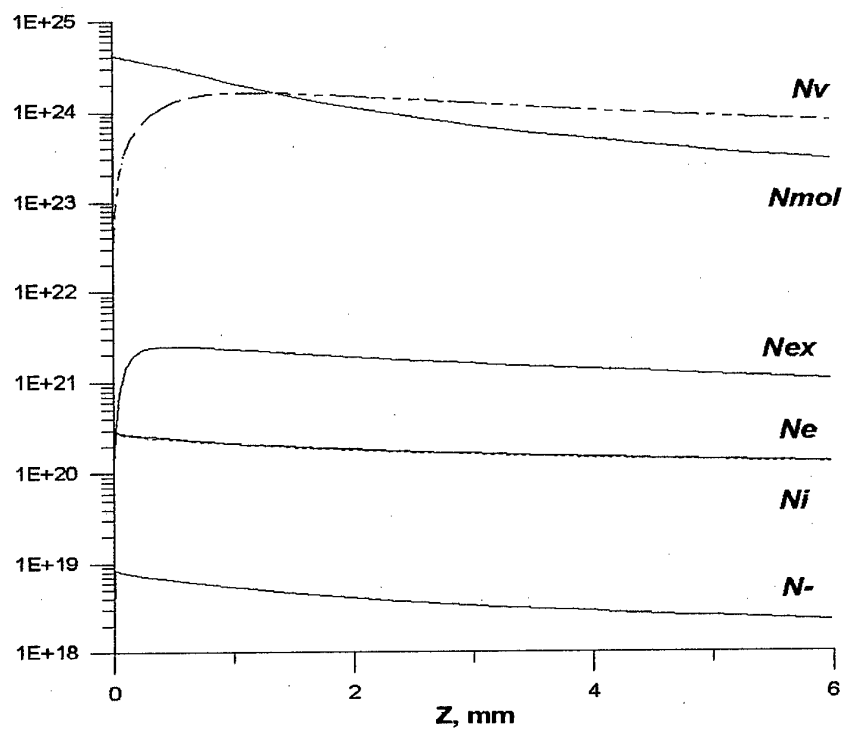
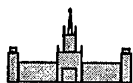


Fig. 3.11. Concentrations of particles, m^{-3} , at $T = 160$ K, $p = 70$ Torr

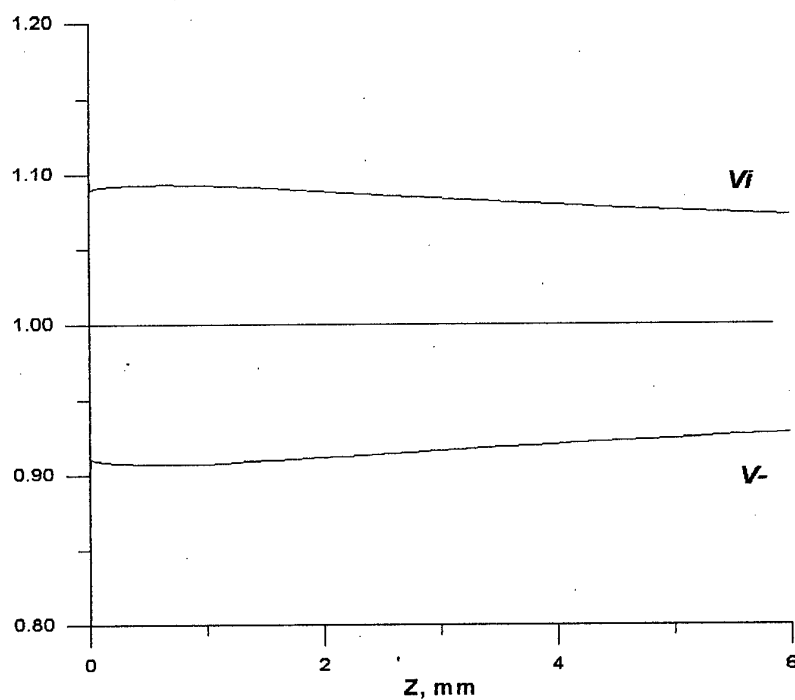


Fig. 3.12. Relative speed of positive and negative ions at $T = 160$ K, $p = 70$ Torr

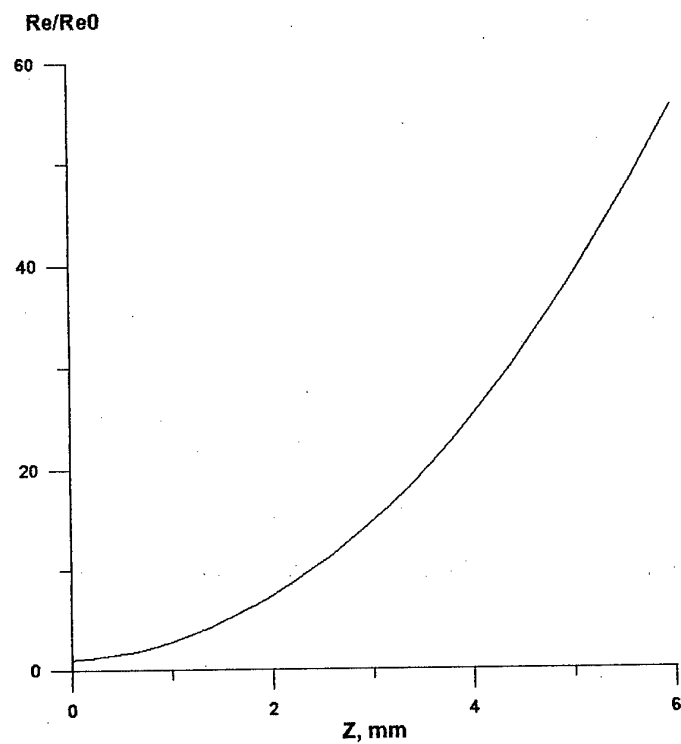
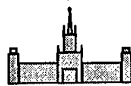


Fig.3.13 Reynolds number spatial distributions (relative units)

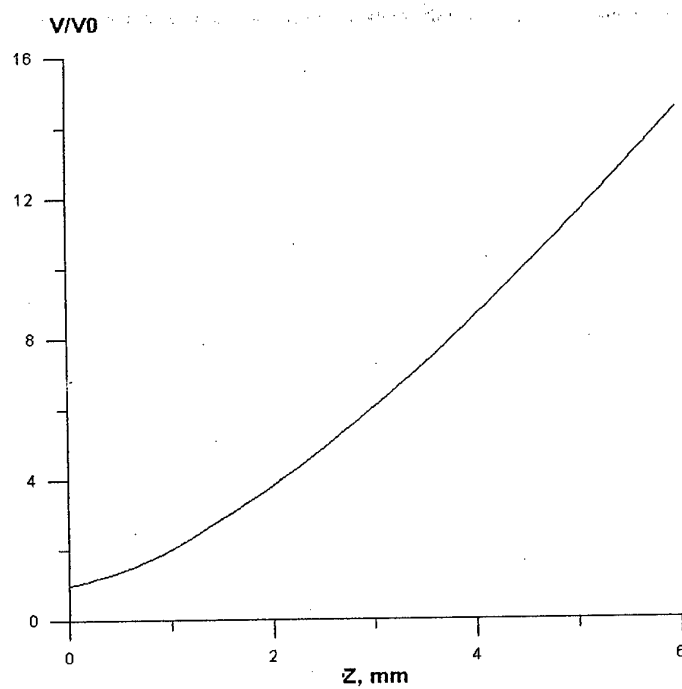


Fig.3.14. Specific volume spatial distribution (relative units)

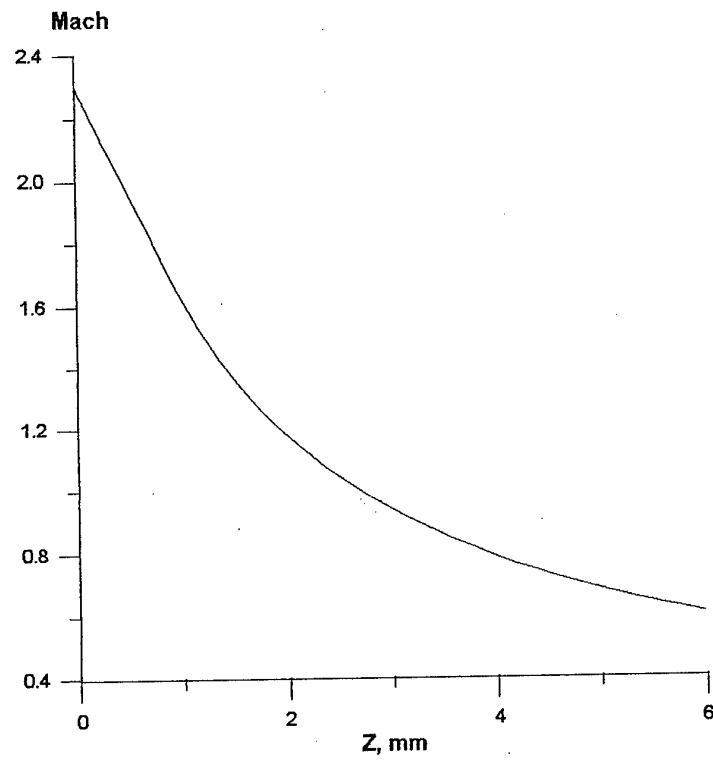
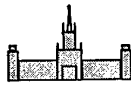
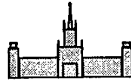


Fig.3.15. Mach number spatial distribution



volume of the discharge. Relative rates of change of all the plasma parameters are much less there.

Speed of ion drift is about an order of magnitude less than the speed of airflow. It means that if one changes electrode polarity (so that the positive ions would be forced to move upstream), the discharge voltage should be enhanced.

Considerable gas heating takes place. Local Mach number changes from initial $M = 2.3$ to $M < 1$, i.e. the flow in the discharge column, according to these results, can become subsonic.

There takes place a multiple growth of plasma viscosity, that can cause a considerable delay of turbulent transition and reduction of viscous component of drag.

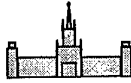
One should note that the ratio of field over gas concentration F/n_m changes are much weaker than for most of the other plasma parameters (by the way, the field is higher in the first region, but F/n_m is less there).

Electron concentration also changes rather weakly. It means that if one neglects variations of electron concentration, it is possible to consider the plasma conductivity to be in inverse proportion to the gas concentration. This approximation is used for the first approach to calculate field and gas dynamics of flow over a model at gas discharge (see below).

The coefficients F_v and F_{ex} (that describe the influence of deviations of the electron distribution functions from equilibrium on excitation of vibration and electron states) grow from 0.2...0.4 to $\cong 1$, while F/n_m is approximately the same. It is a result of the fact that plasma parameters deviate from those characteristic for steady state at given F/n_m .

3.3. Plasma dynamics and current distribution at discharges in flow over a body

Main assumption for the first job is that energy is effectively transported from various excited states (primarily vibrations and dissociation) to gas translation and rotation degrees



of freedom. We also simplify the volume processes of free electrons birth and disappearance. In such a case electron temperature magnitude does not effect on results, so we can take it to be constant. At further progress we shall gradually switch on the previously neglected effects. We denote with O_i places where these effects will contribute, at first job $O_i=0$ for all i .

Gas dynamics:

Mass conservation

$$\partial n_g / \partial t + \text{div}(n_g \mathbf{v}_g) = 0,$$

momentum conservation

$$\rho_g d\mathbf{v}_g/dt = -\text{grad} p_g + O_1 + q,$$

here for q we take now the value necessary for shocks computation only,

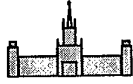
translation and rotation energy conservation

$$\begin{aligned} n_g dE_g/dt &= -p_g \text{div} \mathbf{v}_g + (1 - O_2) j^2 / \sigma, \\ n_g &= n_m + 0.5 n_a, \quad \rho_g = n_g m_m, \quad p_g = (n_m + n_a) T_g, \\ E_g &= T_g (5/2 n_m + 3/2 n_a) / n_g, \quad n_a = O_3. \end{aligned}$$

The boundary conditions for these equations are rather traditional for flow over a body consideration - gliding on the walls and the axis, and free entry and exit before and after the body.

Electromagnetic field is determined from the following equations:

$$\begin{aligned} \partial \mathbf{B} / \partial t &= \nabla [1/(\mu_0 e n_e \dot{\mu}_e)] \nabla \mathbf{B} + \text{rot} [\mathbf{v}, \mathbf{B}], \\ \mathbf{j} &= \text{rot} \mathbf{B} / \mu_0, \quad \mathbf{F} = \mathbf{j} / \sigma. \end{aligned}$$



According to the results of study of plasma processes (see above), plasma concentration and electron temperature can be considered to be constant. The latter corresponds to no account to plasma concentration alteration due to ion diffusion and drift relatively the gas, and supposition that volume ionization and recombination processes are also negligible in comparison with emission from the anode and cathode layers. Emission intensity (i.e. electron concentration) was determined so that to achieve approximate equality of experimental and numerical values of the discharge voltage and current. Then conductivity σ distribution is determined by electron mobility

$$\begin{aligned}\mu_e &= e/(v_{el}m_e), \quad v_{el} = \sigma_{el} v_{eT} n_m + \sigma_{ee} v_{eT} n_e + \sigma_{ei} v_{eT} n_e, \\ v_{eT} &= (2T_e/m_e)^{1/2}, \\ \sigma_{ee} &= 16 \pi a_0^2 (2 \cdot 27.2/T_e)^2 \ln \Lambda_e, \quad \ln \Lambda_e = 23 + 1.5 \ln(T_e) - 0.5 \ln n_e, \\ \sigma_{ei} &= \sigma_{ee} / 2^{1/2},\end{aligned}$$

here cross section for elastic collisions σ_{el} is known from experiments. For the conditions of plasma aerodynamic experiments the first term dominates in the formula for v_{el} , i.e. $\sigma \sim 1/n_m$.

The boundary conditions for this equation are: $B(r = r_{\max}) = 0$ - for the axis and big radii, including walls behind the electrodes (BAHGFE, see fig. 3.16), $B(r) = I/(2\pi r)$ - for walls between the electrodes (CD), here I is the total current. On the electrodes surfaces (BC and DE) in reality there are cathode and anode boundary layers with complicated three-dimensional structure. We shall not consider it in this work. Usual conditions - zero F tangent components near the metallic surfaces - are used.

The discharge regime corresponded to that examined experimentally and numerically (at plasma kinetic computations, see above). The model had a conic frontal surface and a thick spike with a long metal sharp conic tip.

A free Lagrangian method based on totally conservative difference schemes and triangular adaptive mesh [78] was used. At modeling the discharge current was growing from zero to the necessary stationary level for about a millisecond, the computations continued until achievement of the quasi stationary regime.

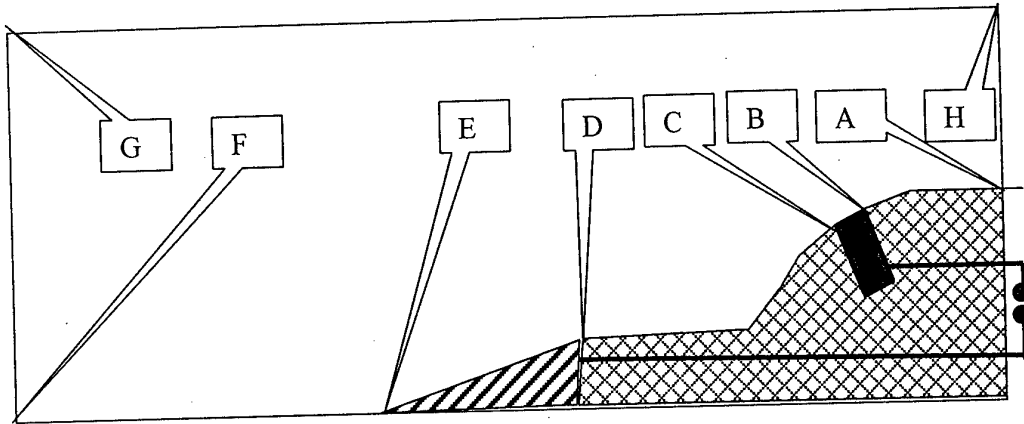
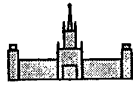
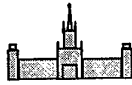


Fig.3.16. On boundary conditions determination



Characteristic results are shown on fig. 3.17 - 3.26.

Three shock waves and corresponding pressure maxims are observed that are formed: 1 - by the conic spike's tip; 2 - by the conic surface of the model itself; 3 - by a "plasma body" formed by the discharge column. The "plasma body" formation takes place because the cold gas cannot enter the region of energy input without heating and pressure gain, which prevents the next portions of cold gas from entering this region. Its formation results in a considerable redistribution of pressure in comparison with a standard flow over the same model with no discharge; the total axial force that yields the wave drag

$$F = \int p \, dA$$

is somewhat less ($\approx 10\%$) than that at the standard flow (here dA is a vector element of the model's surface).

Electric field maximum is situated at the critical point (on the spike) due to the well-known effect of field concentration near sharp tips. However there is practically no current there, as the air is too dense and cold around the tip. Another, much weaker local field maximum is near the hind end of the frontal electrode, just before the discharge column. The latter field maximum provides breakdown of the cold dense air. In the whole, the electric field distribution does not differ significantly from that of a case of zero airflow conductivity and no current. It is a result of comparatively low level of plasma conductivity at the present plasma aerodynamic experiments.

Main current distribution is situated near the model's surface, where the gas density is low, and plasma conductivity is higher than anywhere else. A much weaker current leaks also from the spike's tip where the electric field is high enough; this effect is possibly overestimated in this model, but it is still quite possible because the air breakdown conditions are met near the critical point.

The Joule heating is concentrated primarily at the hind end of the frontal electrode, on the upstream end of the plasma discharge channel. It provides a quick growth of gas temperature.

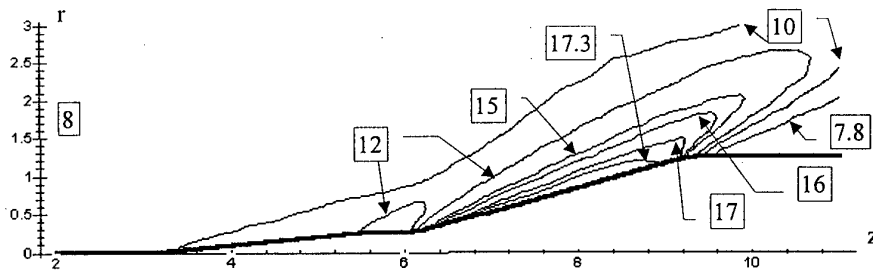
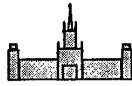


Fig. 3.17. Pressure distribution, kPa, at initial airflow Mach number 2.3, pressure 8 kPa, temperature 160 K, with no current

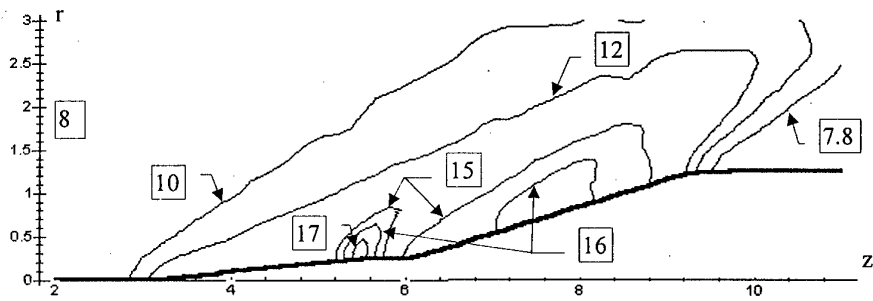


Fig. 3.18. Pressure distribution, kPa, at initial airflow Mach number 2.3, pressure 8 kPa, temperature 160 K, current 2 A

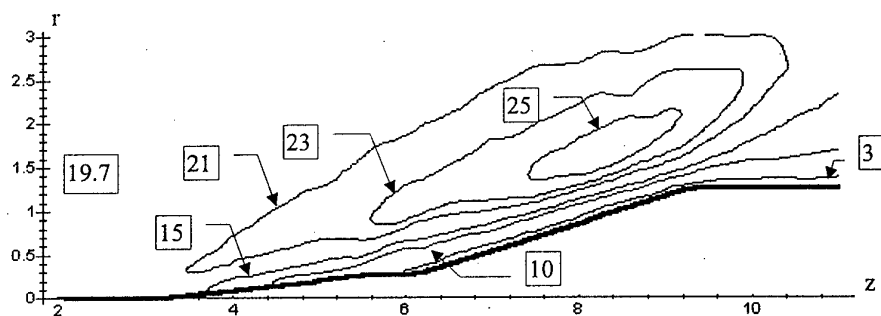


Fig. 3.19. Density distribution, 10^{-2} kg/m^3 , at initial airflow Mach number 2.3, pressure 8 kPa, temperature 160 K, current 2 A

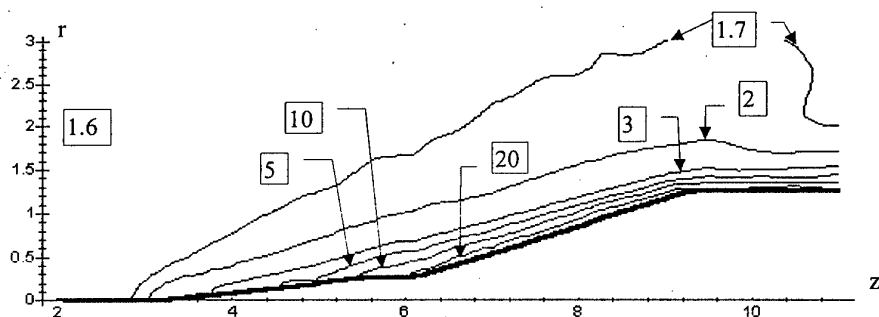


Fig. 3.20. Temperature distribution, 100 K, at initial airflow Mach number 2.3, pressure 8 kPa, temperature 160 K, current 2 A

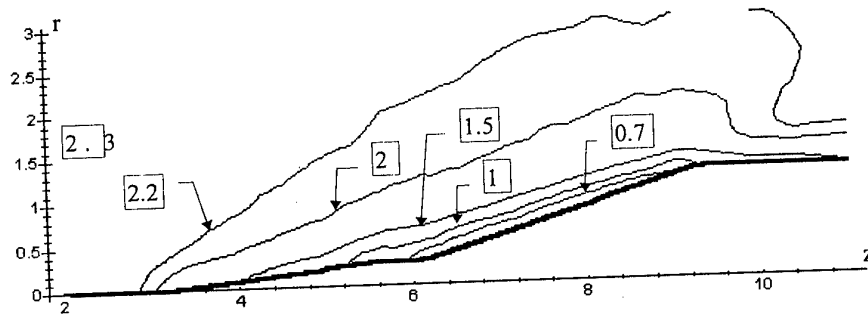
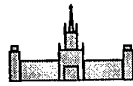


Fig. 3.21 Local Mach number distribution at initial airflow Mach number 2.3, pressure 8 kPa, temperature 160 K, current 2 A

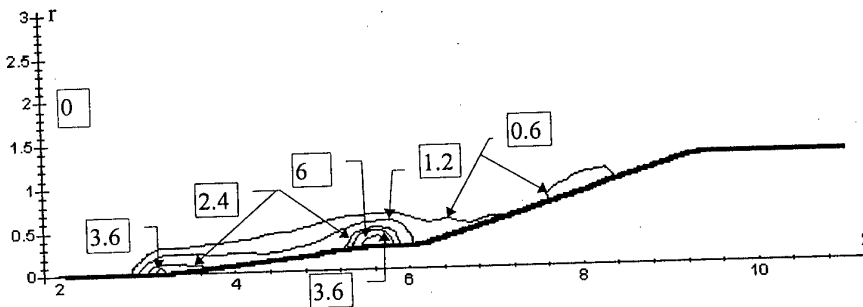


Fig. 3.22. Joule heating power distribution, GW/m^3 , at initial airflow Mach number 2.3, pressure 8 kPa, temperature 160 K, current 2 A

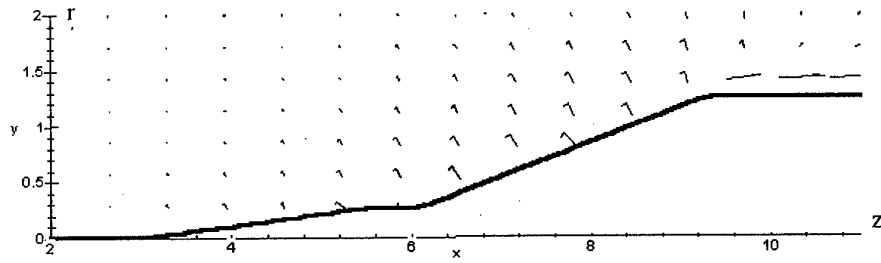
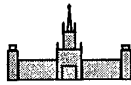


Fig. 3.23. Gas velocity at initial airflow Mach number 2.3, pressure 8 kPa, temperature 160 K, current 2 A

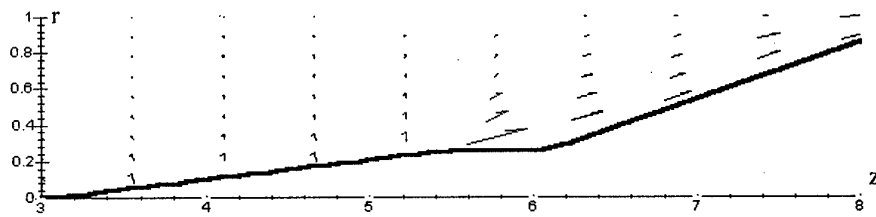


Fig. 3.24. Electric current distribution near the frontal electrode at initial airflow Mach number 2.3, pressure 8 kPa, temperature 160 K, current 2 A

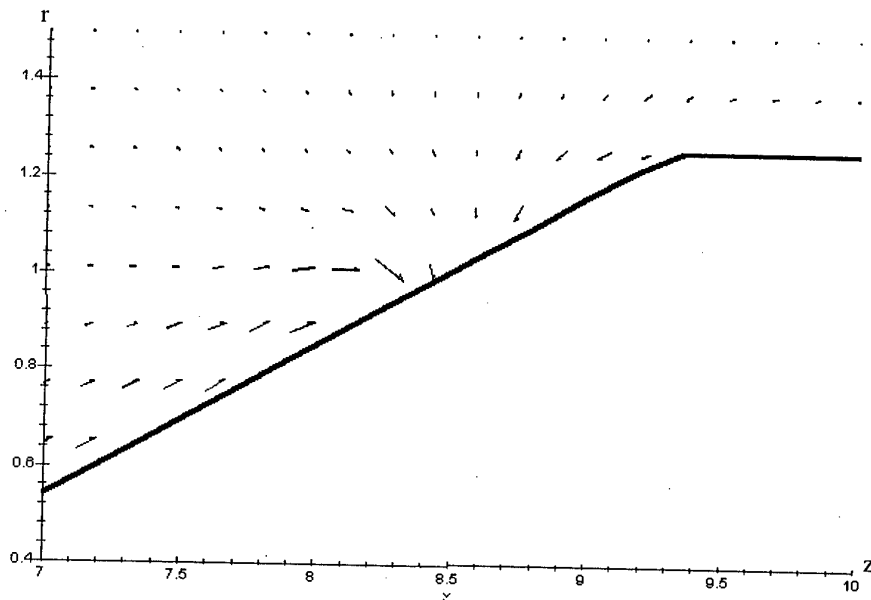
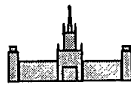


Fig. 3.25. Electric current distribution near the hind electrodes at initial airflow Mach number 2.3, pressure 8 kPa, temperature 160 K, current 2 A

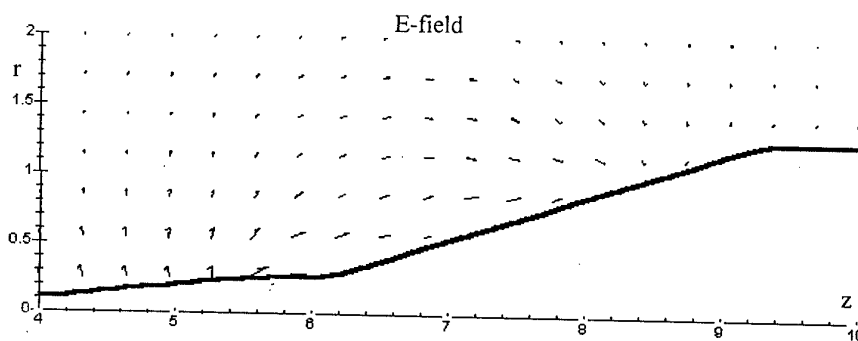
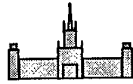


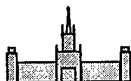
Fig. 3.26. Electric field distribution at initial airflow Mach number 2.3, pressure 8 kPa, temperature 160 K, current 2 A



Heating is much weaker downstream, so the gas temperature in an elementary portion of air does not rise as it passes along the channel. Note that it coincides with the experiments that expose high gas temperatures in all the interelectrode gap. The experiments also show that gas temperature passes a maximum and falls downstream the discharge channel; this fall might be a result of turbulent heat transfer that has not been taken into account at present studies.

One can also see a smaller maximum of Joule heating near the spike's tip, but its total power is small enough (pay account to the axial symmetry of the graphs). Its influence on gas specific energy, temperature and density distributions is comparatively insignificant. This might cause the fact that no intense radiation is observed experimentally near the spike's tip, though the numerical results show that a part of discharge current can leak from there.

Local Mach number on a part of the model's surface is less than 1 (i.e. the flow is locally subsonic). It is a result of considerable gas heating by the discharge. However this fact seems not to affect distributions of pressure, velocity and other gas dynamic parameters.



4. General Consideration of Results

At job formulation for the present studies, we had relied upon previous results of Dr. Klimov at al (private communication and talks in the MSU), which said that the plasma region is quasi steady, axially symmetrical and covers all the interelectrode gap. These conclusions have proved to be based on photographs and shadow photographs with long exposition time and poor focusing of optics. The discharge differs greatly from its previous description.

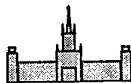
In the best experimental series the discharge between the frontal spike and the hind sectioned electrode had a form of one longitudinal channel between the spike and one of the 8 sections, and a series of transversal channels between these sections. It is a result of plasma thermal instability, it is inevitable at present gap construction and flow parameters. In most cases the shear flow instability is to take place; it is seen from both our experimental and numerical studies. It gives rise to turbulent heat and momentum transfer.

These instabilities result in unsteady character of the phenomenon in the whole.

One more aspect which importance had been underestimated is a dramatic erosion of both model's surface and electrodes (especially at effective regimes with high energy input into the plasma region). A considerable part of the discharge plasma is composed of erosive matter, that can differ plasma properties significantly.

However in most cases shortcuts took place, and either all the discharge was observed inside the model, or a transversal ring discharge between the hind electrodes was registered. It is a result of unoptimal design of the plasma generators.

That is why the diagnostic and numerical methods which were used by us in this study have proved to be not so adequate as we had expected. The diagnostic set up had a very long characteristic time. That is why the experimental data are not very accurate, and they do not provide a thorough description of the airflow with discharge. The numerical models did not



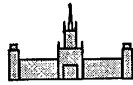
pay account to turbulence and the three-dimensional discharge geometry. The two theoretical approaches also have further shortcuts, for each of them considers the phenomenon from one of the two aspects (plasma processes or magnetic gas dynamics), while their interaction is strong and nonlinear, and an adequate model must take into account both of the aspects.

However, a unanimous analysis of all the experimental and theoretical data with respect to their accuracy has resulted in the following conclusions that we consider to be reliable.

Under conditions of the plasma aerodynamic experiments, plasma state is very far from equilibrium: vibration is excited in a major part of molecules, a considerable number of electronically excited molecules is generated, electron energy distribution function deviates from the equilibrium one (especially in the region of major energy input). It results from spectral measurements of T_v and T_g and from plasma computations.

Computation of plasma processes on base of the present state of plasma physics shows that electron pressure, ion-molecule friction force, ion sound effects on the gas flow are negligible for the present experimental conditions (due to low concentration of the charged particles relatively the neutral molecules).

Plasma processes of energy distribution from electric field to various energy reservoirs are non-linear and change the whole flow over the model considerably, they cannot be expressed in terms of linear uniform heating in a current channel. The region of electric energy input into plasma is situated in the vicinity of the frontal electrode (more accurately, near its downstream end), this region has a quasi spherical shape, and rather a small volume. Energy input along the rest of the current channel is much smaller due to much higher plasma conductivity (because the neutral gas concentration is much less there). That is why the gas multiple heating at the frontal part of plasma channel is very intensive. It results from the both numerical researches (plasma and gas/field approaches), and corresponds to the measured temperature longitudinal distributions (T_g quickly rises from initial cryogenic temperature to ~ 1000 K, further relative changes of the measured and computed temperature is much weaker).

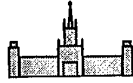


Gas heating rate distribution differs from the energy input distribution, the heating takes place in all the plasma region. It results from nonlinear character of processes of energy redistribution from vibration and excitation energy reservoirs, as well as from thermal effects of various plasma chemical reactions. At plasma processes modeling (at uniform longitudinal distributions of pressure and speed) it gives a continuous temperature growth. At the MHD computation, plasma flow acceleration is here accompanied by fall of translation temperature. Experiments expose still more effective fall of gas temperature behind its maximum situated near the energy input maximum (as a result of unanimous effect of turbulent heat transfer and acceleration).

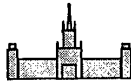
The energy input region is flown over with a strong shock wave formation in the airflow, and with the corresponding pressure gain in the plasma region. If there is enough space, i.e. the model «forehead» with the shock wave structure is far enough from the region of electric energy input, a plasma jet is generated at expansion of the compressed plasma. This jet flows over the model with speed that sufficiently exceeds the speed of airflow. It prevents a considerable reduction of the wave drag. Shear on the interface plasma – cold air may cause turbulence generation. Those conclusions are based primarily on the MHD modeling, a shock wave at the downstream end of the frontal electrode and turbulence at the plasma – gas interface are registered experimentally.

Considerable gas heating is observed, molecular translation temperature rises up to 1...2 kK. That is why for some regimes the plasma jet is subsonic, which results in uniform pressure distribution in plasma, and in absence of shock waves in the plasma region. The corresponding Reynolds numbers are much lower than for the same flow without the discharge, which may delay the laminar-turbulent transition and thus reduce the viscous drag. High gas temperature is present in the both numerical approaches and in experimental results.

The best registered drag reduction in these experiments with the instable three-dimensional discharges is still rather considerable (15% for the model with the spherical frontal part, and 10% for the conic model). Note that the axisymmetrical MHD computations also show 10% wave drag reduction for the conic model, and the turbulent friction reduction must be added

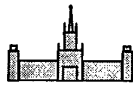


to this numeral. It shows that at proper discharge organization the effect of drag reduction can be significantly enhanced.



Conclusions

1. The present researches have shown that formation of weakly ionized strongly nonequilibrium plasma in supersonic airflow near a surface of a model may improve its aerodynamic characteristics, it has a good prospect of application in aerodynamics, especially at high Mach numbers. The next efforts in this direction are to be bound with the following problems:
 - A. Proper organization of discharge processes, including control and minimization of erosion of electrodes and surfaces, elimination of shortcuts etc.
 - B. Optimization of geometrical characteristics of the electrodes and the interelectrode gap, so that to minimize plasma instabilities effect on the discharge's structure.
 - C. Investigation of the discharge structure and its dynamic characteristics with a sufficiently high spatial and temporary resolution.
 - D. Revealing the basic mechanisms that yield the drag reduction, and their optimization.
2. The most important events seem to happen in a comparatively thin boundary layer near the model's surface, and on the surface itself. That is why it is necessary to answer the following questions:
 - A. What are the mechanisms that modify the surface in a way that the aerodynamic properties of the model keep improved for a long time after the discharge, even at comparatively weak erosion (see fig. 14 - relaxation of drag to a new value).
 - B. How does plasma formation affects the interaction of the model's surface and the airflow during the discharge (including pressure and tangent viscous forces in the boundary layer, its size and hydrodynamic stability, etc.) - with respect to the



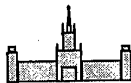
processes that result in changes in the structures of both the plasma boundary layer and the surface.

3. The phenomenon under investigation is rather difficult for diagnostics, and it is unlikely to get all the necessary information on base of experiments only. It is apparently much easier to achieve the goals mentioned above on base of a complex experimental and numerical research with a detailed analysis of all the results. The following efforts should be undertaken.

A. Combination of the two theoretical models used in the present work into one, taking into account both MHD and plasma chemical processes in the discharge volume.

B. Account of three-dimensional aspects of the discharge structure.

C. Creation of theoretical models that would describe the plasma boundary layer structure, plasma-surface interaction, and processes on the surface that yield its modification during the discharge and drag reduction after its quenching.



References

1. Klimov A.I., Koblov A.M., Mishin G.I. Propagation of shock waves in a glow discharge plasma. //Pis'ma v Zhurnal Tekhnicheskoi Fiziki. 1982.V.8.N.7. P.349-344. (In Russian).
2. Gorshkov V.A., Klimov A.I., Mishin G.I. et al. Peculiarities of electron density behavior in weakly ionized non equilibrium plasma at propagation of shock wave in it. //Zhurnal Tekhnicheskoi Fiziki. 1987.V.57.N.10. P.1893-1898. (In Russian).
3. Mishin G.I., Klimov A.I., Gridin A.Yu. Measurements of pressure and density in shock waves in a gas discharge plasma. //Pis'ma v Zhurnal Tekhnicheskoi Fiziki. 1991.V.17.N.16. P.84-89. (In Russian).
4. Evtiukhin I.V., Margolin A.D., Shmelev V.M. On nature of acceleration of shock waves in a glow discharge plasma. //Khimicheskaya Fizika. 1984. V.3. N.9. P.1322-1327. (In Russian).
5. Voinovich P.A., Ershov A.P., Ponomareva S.E., Shibkov V.M. Propagation of weak shock waves in longitudinal glow discharge plasma of air. //Teplofizika Vysokhikh Temperatur. 1991. V. 29. N.3. P.582-590.; Propagation of a shock waves in a plasma of glow discharge in air. Preprint of Ioffe Physics Technical institute. Leningrad. 1990. N. 1453. (In Russian).
6. Chiutov Yu.I., Podolskii V.N., Braion D.A. Blast waves developing in a gas discharge. //Pisma v Zhurnal Tekhnicheskoi Fiziki. 1991.V.17.N.3. P.59-62. (In Russian).
7. Chiutov Yu.I., Podolskii V.N., Braion D.A. Blast wave in thermal non uniformity in a gas discharge argon plasma. In Collection of reports 2nd All Union scientific seminar "Interaction of acoustic waves with a plasma". Erevan. 1991. P.99-101. (In Russian).
8. Basargin I.V., Mishin G.I. Probe measurements of shock waves in a plasma of a transverse glow discharge. //Pis'ma v Zhurnal Tekhnicheskoi Fiziki. 1985.V.11.N.21. P.1297-1303. (In Russian).
9. Kim A.E., Raevskii D.K. Propagation of a shock wave through the region of heated gas. //Preprint IVTAN n. 2-250. M., 1988. (In Russian).
10. Bystrov S.A., Ivanov V.I., Shugaev F.V. Propagation of a flat shock wave in weakly ionised plasma. //Fizika Plasmy. 1989. V.15. N.5. C.558-562. (In Russian).
11. Ershov A.P., Klishin S.V., Kuzovnikov A.A. et al. Application of reduction method to RF interferometry of shock waves in a weakly ionised plasma. //Zhurnal Tekhnicheskoi Fiziki. 1989.V.59.N.8. P.142-145. (In Russian).
12. Grachev L.P., Esakov I.I., Mishin G.I. et al. Interaction of shock wave with a decaying plasma of an electrodeless RF discharge. //Zhurnal Tekhnicheskoi Fiziki. 1985.V.55.N.5. P.972-975. (In Russian).



13. Aleksandrov A.F., Vidiakin N.G., Lakutin et al. On the possible mechanism of shock wave interaction with a decaying plasma of a laser spark in air. //Zhurnal Tekhnicheskoi Fiziki. 1986.V.56.N.4. P.771-774. (In Russian).
14. Barkhudarov E.M., Beresovskii V.R., Mdivnishvili N.O. Dissipation of a weak shock wave in a laser spark in air. //Pis'ma v Zhurnal Tekhnicheskoi Fiziki. 1984.V.10. N.19. P.1178-1181. (In Russian).
15. Babaeva N.Yu., Mnatsakanyan A.Kh., Naidis G.V. Simulation of a shock wave propagation in a developing gas discharge in nitrogen. //Teplofizika Vysokhikh Temperatur. 1993. V. 31. N.4. P.670-673. (In Russian).
16. Kamrukov A.S., Kozlov N.P., Protasov Yu.S., Chuvashhev S.N. Radiatsyonno-Plazmodinamicheskiye Effekty v Kumulyativnykh Plazmodinamicheskikh Razryadah (Radiation and Gas Dynamic Effects that Take Place at Cumulative Plasmadynamic Discharges). //Zhurnal Tekhnicheskoi Fiziki (Sov.Physics: Technical Physics). 1985. V.55. N.3. P.533-543. (In Russian).
17. Avramenko R.F., Rukhadze A.A., Teselkin S.F. On the structure of a shock wave in a weakly ionized, non isothermal plasma. //Pis'ma Zh. Eksp.Teor. Fiziki. 1981.V.34. N.9. P.485-488. (In Russian).
18. Rukhadze A.A., Teselkin S.F. On the structure of the disturbance of a weakly ionized plasma at a discontinuity movement of neutral component. //Zhurnal Tekhnicheskoi Fiziki. 1982.V.52.N.11. P.2129-2133. (In Russian).
19. Teselkin S.T. Diffusion precursor of a shock wave in weakly ionized plasma of electronegative gas. //Pisma v Zhurnal Tekhnicheskoi Fiziki. 1991.V.17. N.16. P.50-55. Teselkin S.T. in a collection of works: Kinetic and gas dynamic processes in non equilibrium media. /Ed. A.M.Prokhorov. M. MSU publishers. 1986. P.99. (In Russian).
20. Pavlov V.A. On the structure of ion-sound shock wave in a weakly ionized plasma. //Fizika Plasmy. 1996. V.22. N.2. C.182-187. (In Russian).
21. Ershov A.P., Klishin S.V., Kuzovnikov S.V., Ponomareva S.E. et al. //Teplofizika Vysokhikh Temperatur. 1990. V. 28. N.6. P.1041-1047. (In Russian).
22. Alferov V.I., Dmitriev L.M. Electric discharge in a flow at the existence of density gradients. //Teplofizika Vysokhikh Temperatur. 1985. V. 23. N.6. P.677-682. (In Russian).
23. Naidis G.V. Spatial distribution of plasma parameters near a shock wave front in a gas discharge. //Teplofizika Vysokhikh Temperatur. 1991. V. 29. N.1. P.15-20. (In Russian).
24. Bychkov V.L., Grachev L.P., Esakov I.I., Deriugin A.A. et al. Numerical and experimental investigation of supersonic flow around blunt body at the existence of the longitudinal discharge. //Preprint Keldysh Institute of applied mathematics. Moscow. 1996. (In Russian).



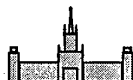
25. Kochetov I.V., Pevgov V.G., Polak L.S., Slovetskii D.I. Plasma Chemical reactions./ Ed. Polak L.S. Moscow: Institute of Petrol and Chemical Synthesis. AS USSR, 1979. (In Russian).
26. Islamov R.Sh., Kochetov I.V., Pevgov V.G. Analysis of processes of interaction of electrons with oxygen molecule. //Preprint Lebedev Physics Institute AS, N. 169, 1977. (In Russian).
27. Aleksandrov N.L., Vysikailo F.I., Islamov R.Sh., Kochetov I.V. et al. Electron distribution function in a mixture $N_2 - O_2 = 4:1$. //Teplofizika Vysokhikh Temperatur. 1981. V. 19. N.1. P.22-27. (In Russian).
28. Aleksandrov N.L., Konchakov A.M., Son E.E. Electron distribution functions and kinetic coefficients of nitrogen plasma. //Fizika Plasmy. 1978. V.4. N.5. P.1182-1186. (In Russian).
29. Akishev Yu.S., Deriugin A.A., Kochetov I.V., Napartovich A.P. et al. Effectiveness of generation of chemically active particles in a self maintained glow discharge. //Fizika Plasmy. 1994. V.20. N.6. P.585-592. (In Russian).
30. Eliasson B., Kogelschatz U. Basic Data for Modelling of Electric Discharge in Gases: Oxygen. Asea Brown Boveri Forschungszentrum CH-5405, Baden, KLR 86-11C, June 1986. V.2. P.1.
31. Yousfi M., Azzi N., Segur P. et al. Electron-molecule collision cross sections and electron swarm parameters in some atmospheric gases (N_2 , O_2 , CO_2 and H_2O). Centre de Physique Atomique de Toulouse & Instituto di Elettrotecnica ed Elettronica Universita di Padova, 1987. P.1.
32. Ellis H.W., Pai R.Y., McDaniel E.W. et al. Transport properties of gaseous ions. Atomic Data and Nuclear Data Tables.1976.V.17.N.3. P.182-210.
33. Akishev Yu.S., Deriugin A.A., Karalchik V.B., Kochetov I.V. et al. Experimental investigation and numerical simulation of constant current glow discharge of atmospheric pressure. //Fizika Plasmy. 1994. V.20. N.6. C.571-584. (In Russian).
34. Evtiukhin I.V., Margolin A.D., Shmelev V.M. Interaction of shock waves in a gas with excited vibrations. //Khimicheskaya Fizika. 1985. V.4. N.9. P.1276-1280. (In Russian).
35. Naidis G.V., Rumyantsev S.V. On the movement of a shock wave through the heat non uniformity. //Teplofizika Vysokhikh Temperatur. 1987. V. 25. N.2. P.389-390. (In Russian).
36. Basargin I.V., Mishin G.I. Propagation of shock waves in a plasma of a transverse discharge in argon. //Pis'ma v Zhurnal Tekhnicheskoi Fiziki. 1985.V.11. N.4. P.209-215. (In Russian).
37. Voinovich P.A., Fursenko A.A., Yuferov A.A. Simulation of interaction of shock waves in gases with spatial non uniformity of parameters. //Preprint of Ioffe Physics Technical institute. Leningrad. 1989. N. 1321. (In Russian).



38. Mnatsakhanyan A.Kh., Naidis G.V., Rumyantsev S.V. Dynamics of air flow at pulse power input to the spherical region with taking into the account vibrational-translational non equilibrium. //Zhurnal Prikladnoi mekhaniki i Tekhnicheskoi Fiziki. 1989. N.6. P. 46-50. (In Russian).
39. Mnatsakhanyan A.Kh., Naidis G.V., Rumyantsev S.V. Shock wave propagation through nonuniform and nonequilibrium gas regions. Proc of 16-th Int. Symp. on Shock Tubes and Waves. Aachen, Germany, 1987, P. 201-205.
40. Vstovskii G.V., Kozlov G.I. Propagation of weak shock wave in vibrationally non equilibrium gas. //Zhurnal Tekhnicheskoi Fiziki. 1986.V.56.N.8. P.1536-1542. (In Russian).
41. Mnatsakhanyan A.Kh., Naidis G.V. Balance of vibrational energy in air discharges. //Teplofizika Vysokhikh Temperatur. 1985. V. 23. N.4. P.640-648. (In Russian).
42. Bychkov V.L., Gureev K.G., Kibovskaya T.T. Steadystates of nitrogen-oxygen mixtures in a non uniform non self maintained gas discharge. //Sov.J. Chem. Phys. 1990.V.7(1). P. 185-195. (In Russian).
43. Gritsynin S.I., Kossyi I.A., Silakov V.P. et al. Long lived plasma in gases of high pressure created by a pulse UV-radiation. //Teplofizika Vysokhikh Temperatur. 1986. V. 24. N.4. P.662. (In Russian).
44. Slovetskii D.I. Mechanisms of chemical reactions in non equilibrium plasma. M. Nauka. 1980. (In Russian).
45. Basiev A.G., Vysikailo F.I., Gurashvili V.A. //Fizika Plasmy. 1983. V.9. N.5. P.1076. (In Russian).
46. Brunet H., Vincent P., Rocca-Serra J. Ionization mechanism in a nitrogen glow discharge. //J. Appl. Phys. 1983. V.54. N.9. P. 4951-4957.
47. Brunet A.G., Rocca-Serra J. Model for a glow discharge in flowing nitrogen. //Ibidem. 1985. V.57. N. 5. P. 1574-1581.
48. Bogdan L.S., Levitskii S.M., Martysh E.V. Non monotonous change of electron concentration in a decaying plasma of pulsed discharge in nitrogen. //Zhurnal Tekhnicheskoi Fiziki. 1983.V.53.N.61. P.203. (In Russian).
49. Vitkovskii V.V., Grachev L.P., Egorova Z.M., Kuznetsov Yu.E. et al. Experimental investigation of electric discharges of continuous current in supersonic and subsonic air flows. Works of TsAGI. N.2505. Moscow. TsAGI publishers. 1991. P. 3-27. (In Russian).
50. A.F.Alexandrov, V.A.Lakutin, M.G.Skvortsov, I.B.Timofeev, V.A.Chernikov. Interaction of Shock Waves with Decaying Laser Spark Plasma in the Air. //Zhurnal Tekhnicheskoi Fiziki. 1986.V.56.N.4. P.771-774. (In Russian).



51. A.P.Ershov, K.Sh.Isaev, I.B.Timofeev. Probe Diagnostics of Last Stages of Dense Plasma Jet Injection into the Atmosphere. //Teplofizika Vysokih Temperatur (High Temperature). V.25, №4, P. 743-747, 1987. (In Russian).
52. A.F.Alexandrov, V.A.Chernikov, I.B.Timofeev. Interaction of shock waves with spatially limited plasma in air 18 ICPIG, Swansea, V.4, P. 618-619, 1987.
53. A.P.Ershov, I.B.Timofeev, S.N.Chuvashev, S.P.Bitskevich. Evolution of Plasma Jet Structure and Parameters at Pulsed Injection into the Atmosphere. //Teplofizika Vysokih Temperatur (High Temperature), 1990. V.28, №3, P.583-589. (In Russian).
54. A.P.Ershov, I.Imad, I.B.Timofeev, S.N.Chuvashev, V.M.Shibkov. High-Speed Plasma Jets in the Air. 1. Dynamics of a Plasma Jet Generated by a Cumulative Conic Shape Plasmatron. //Teplofizika Vysokih Temperatur (High Temperature). 1993, т.31, № 3, с. 364-368. (In Russian).
55. A.P.Ershov, I.Imad, I.B.Timofeev, S.N.Chuvashev, V.M.Shibkov. High-Speed Plasma Jets in the Air. 2. Parameters of a Pulsed Plasma Jet Injected into the Atmosphere by a Cumulative Plasmatron. //Teplofizika Vysokih Temperatur (High Temperature). 1993. V.31. № 4. P. 531-534 (In Russian).
56. A.F.Alexandrov, A.P.Ershov, I.Imad, I.B.Timofeev, S.N.Chuvashev, V.M.Shibkov. High-Speed Plasma Jets in the Air. 3. Non-laser Continuous Optical Discharge in the Atmosphere. //Teplofizika Vysokih Temperatur (High Temperature). 1993. V.31, № 5. P.850-851. (In Russian).
57. A.S.Zarin, A.A.Kuzovnikov, V.M.Shibkov. Svobodno Lokalizovannyi SVCh Razrad v Vozduhe (Freely Localized Microwave Discharge in Air). Moscow: Oil & Gas.1996. 204 p. (In Russian).
58. V.V.Zlobin, A.A.Kuzovnikov, V.M.Shibkov. Concentration of electrons in a stimulated MW discharge channel in nitrogen. //Moscow University Physics Bulletin. Fizika. V.43. No.1. (1988), P.98-100.
59. A.A.Devyatov, A.A.Kuzovnikov, V.V.Lodinev, V.M.Shibkov. The mechanism of molecular gas heating in a pulsed free-localizing RF discharge. //Moscow University Physics Bulletin. Fizika. V.46. No.2. (1991). P.28-31.
60. V.V.Lodinev, V.M.Shibkov, L.V.Shibkova. Gas heating kinetics in pulse-periodic air discharge. //Moscow University Physics Bulletin. Fizika. V.51. No.2. (1996). P.26-31.
61. A.A.Kuzovnikov, V.M.Shibkov, L.V.Shibkova. Free-localized pulse-periodic MW discharge in air. Kinetics of gas heating. //High Temperature. V.34. No.3. (1996). P.343-348.
62. V.M.Shibkov. Free-localized pulse-periodic MW discharge in air. Electric field strength in plasma. //High Temperature. V.34. No.4. (1996). P.519-524.



63. A.A.Kuzovnikov, V.M.Shibkov, L.V.Shibkova. Kinetics of charged particles in a free-localized pulse-periodic MW discharge in air. //High Temperature. V.34. No.5. (1996). P.651-655.
64. A.A.Kuzovnikov, V.M.Shibkov, L.V.Shibkova. Kinetics of Electrons in Plasma of a Discharge Formed in a Free Space by a Focused Microwave Beam. //Zhurnal Tekhnicheskoi Fiziki. 1997. V.67. N.6. P.10-14. (In Russian).
65. A.F.Alexandrov, A.S.Zarin, A.A.Kuzovnikov, V.M.Shibkov, L.V.Shibkova. Parameters of Plasma of a non-selfsustained Microwave Discharge Formed in a Regime of Programmable Pulse. //Zhurnal Tekhnicheskoi Fiziki. 1997. V.67. N.7. P.19-23. (In Russian).
66. V.M.Shibkov. Gas Heating under Conditions of Freely Localized Microwave Discharge in the Air. Mathematical Modeling. //Teplofizika Vysokih Temperatur (High Temperature). 1997. V.35. №5. P.693-701.
67. V.M.Shibkov. Gas Heating under Conditions of Freely Localized Microwave Discharge in the Air. Experiment. //Teplofizika Vysokih Temperatur (High Temperature). 1997. V.35. №6, P.871-875.
68. Spier J.L., Smit-Miessen M.M. On the determination of the temperature with the aid of non-resolved CN bands 3883 and 3871 Å°. //Physica. 1942. V.9. №4. P.422-432.
69. Ochkin V.N. Issledovaniye Fiziko-Himicheskikh Svoistv Plasmi CO₂ - Lasera. (Investigation of Physical and Chemical Properties of CO₂ - laser plasma //Trudi FIAN SSSR (Proc. of Physical Inst. of Acad.Sci.USSR). 1974. V.78. P.3-57.
70. Chan P., Telbot L., Turan K. Electric Probes in Steady and Moving Plasma. M., Mir. 1978. (In Russian).
71. Chen X. //J.Phys.D. Applied Physics. 1982.V.15. P. 1695.
72. Benilov M.S., Rogov B.V., Tirskey G.A. //High Temperature. 1981. V.19. N-5. P.1031. (In Russian).
73. Alexeyev B.V., Kotelnikov V.A. Probe method of plasma diagnostics. Moscow: Energoatomizdat. 1988. (In Russian).
74. Wojaczek K. //Beitr.Plasmaphys., 1965. Bd.5. N 3. P.181.
75. Yu.S.Protasov, S.N.Chuvashev. Fizicheskaya Elektronika Gazorazryadnyh Ustroystv. V.2. Plazmennaya Elektronika (Physical Electronics of Gas Discharges. V. 2. Plasma Electronics). - Moscow: Vysshaya Shkola. 1993. 736 p. (In Russian).
76. Biberman L.M., Vorobiov V.S., Yakubov I.T. Kinetika neravnovesnoy nizko-temperaturnoy plazmy (Kinetics of Non-equilibrium Low Temperature Plasma). Moscow: Nauka.1982. (In Russian).



77. Chuvashov S., Ershov A., Liagushin B., Timofeev B., Timofeev I. Ambient Air Modification for Drag Reduction. Similarity Analysis Results for Modeling of Weakly Ionized Plasma Aerodynamics. // Workshop on Weakly Ionized Gases: Proc. Colorado: USAF Academy. 1997.

78 Ardelyan N.V., Kosmachevskij K.V., Chuvashov S.N. a.o. Chislennoye Modelirovaniye i Teoreticheskiye Issledovaniya Radiatsyonno-Plazmodinamicheskikh Razryadov (Numerical Modeling and Theoretical Studies of Radiating Plasmadynamic Discharges) // In: Radiatsyonnaya Plazmodinamika (Radiating Plasma Dynamics). Moscow: Energoatomizdat. 1991. P. 191-249 (In Russian).

Professor I.B. Timofeev

Department of Physics

Moscow State University

119899, Moscow, Russia

Tel.: 007-095-9393885

Fax.: 007-095-9391787

E-mail: shibkov@ph-elec.phys.msu.su

E-mail: alex@ph-elec.phys.msu.su